JOURNAL OF GEOPHYSICAL RESEARCH, VOL. 111, C07010, doi:10.1029/2003JC002157, 2006

Ocean mixed layer depth: A subsurface proxy of ocean-atmosphere variability

K. Lorbacher,[1,2] D. Dommenget,[1,2] P. P. Niiler,[1] and A. Köhl[1,3]

Received 10 October 2003; revised 10 January 2006; accepted 9 February 2006; published 12 July 2006.

[1] A new criterion, based on the shallowest extreme curvature of near surface layer density or temperature profiles, is established for demarking the mixed layer depth, h_{mix}. Using historical global hydrographic profile data, including conductivity-temperature-depth and expendable bathythermograph data obtained during World Ocean Circulation Experiment, its seasonal variability and monthly to interannual anomalies are computed. Unlike the more commonly used Δ criterion, the new criterion is able to deal with both different vertical resolutions of the data set and a large variety of observed stratification profiles. For about two thirds of the profiles our algorithm produces an $h_{\mathrm{mix}/c}$ that is more reliable than the one of the Δ criterion. The uncertainty for $h_{\mathrm{mix}/c}$ is ± 5 m for high- (<5 m) and ± 8 m for low- (<20 m) resolution profiles. A quality index, $\mathrm{QI}_{\mathrm{mix}}$, which compares the variance of a profile above h_{mix} to the variance to a depth of $1.5 \times h_{\mathrm{mix}}$, shows that for the 70% of the profile data for which a clearly recognizable well-mixed zone exists near the surface, our criterion identifies the depth of the well-mixed zone in all cases. The standard deviation of anomalous monthly $h_{\mathrm{mix}/c}$ is typically 20–70% of the long-term mean $h_{\mathrm{mix}/c}$. In the tropical Pacific the monthly mean anomalies of $h_{\mathrm{mix}/c}$ are not well correlated with anomalies of sea surface temperature, which indicate that a variety of turbulent processes, other than surface heat fluxes, are important in the upper ocean there. Comparisons between observed $h_{\mathrm{mix}/c}$ and Massachusetts Institute of Techonology/ocean general circulation model/Estimating the Circulation and Climate of the Ocean model simulated mixed layer depth indicate that the *K*PP algorithm captures in general a 30% smaller mixed layer depth than observed.

Citation: Lorbacher, K., D. Dommenget, P. P. Niiler, and A. Köhl (2006), Ocean mixed layer depth: A subsurface proxy of ocean-atmosphere variability, *J. Geophys. Res.*, *111*, C07010, doi:10.1029/2003JC002157.

1. Introduction

[2] The mixed layer of the ocean is commonly considered as the region near its surface with vertically quasi-uniform oceanic tracers (temperature, salinity and density) above a layer of more rapid vertical changes. The intense vertical turbulent mixing near the surface penetrates a short distance into the top of the pycnocline and is the cause of the observed vertical uniformity. The vigorous vertical turbulence is generated mainly by the action of the horizontal momentum and the vertical buoyancy fluxes derived from the atmospheric energetic motions. Variations of these fluxes are well documented [e.g., *Kalnay et al.*, 1996; *Roads et al.*, 2003] and these force variations of the mixed layer depth, h_{mix}, on daily to interannual timescales. The heat budget of h_{mix} is of particular interest because it governs the evolution of the sea surface temperature (SST), which is the most important ocean parameter influencing the atmosphere. It is important to know not only the SST evolution but also how deep the homogeneous thermal energy column penetrates into the stratified ocean. The main objectives of this paper are to present a new computation of the global distribution of h_{mix}, to verify the skill of this method based on both global observations and the output of ocean general circulation models (OGCMs) and to analyze the effect of h_{mix} anomalies on seasonal-to-interannual ocean-atmosphere interaction.

[3] As a point of departure, consider the global coupled atmosphere-ocean model of *Alexander et al.* [2000]. In its locally one-dimensional upper ocean h_{mix} is time dependant and there is a flux of thermal energy out of the bottom of the mixed layer. According to *Alexander et al.* [2000] the evolution of SST anomalies, $\delta(\mathrm{SST})$, is dominated by three terms:

$$\frac{d}{dt}\delta(\mathrm{SST}) \approx \frac{\delta(F)\overline{\eta}}{c_p\rho} + \frac{\overline{F}\delta(\eta)}{c_p\rho} + \delta(w_e)\overline{\Delta T \eta}, \qquad (1)$$

where $h_{\mathrm{mix}} \equiv 1/\eta$, overbars define a temporal mean, and $\delta(\,)$ defines the departures from the mean; c_p is the specific heat and ρ the density of seawater. The entrainment heat flux is

[1] Scripps Institution of Oceanography, La Jolla, California, USA.
[2] Now at Leibniz Institute of Marine Sciences at University of Kiel (IFM-GEOMAR), Kiel, Germany.
[3] Now at Institut für Meereskunde, Hamburg, Germany.

0148-0227/06/2003JC002157$09.00

proportional to the product of the entrainment rate w_e and the temperature jump at the base of the mixed layer ΔT. Therefore changes in δ(SST) are forced by the time integration of highly energetic short-term anomalous variations of surface fluxes, $\delta(F)$, the entrainment rate at the base of the mixed layer and, of capital importance for this study, anomalous h_{mix}.

[4] *Dommenget and Latif* [2002] point out that the variability of h_{mix} on seasonal to longer timescale should also be an important parameter to consider in climate model diagnostics. In our context the second term on the right hand side of equation (1) gives a direct way to estimate the sensitivity of SST evolution in an anomalous h_{mix} field. A monthly mean $\delta(h_{\mathrm{mix}})$ anomaly during midlatitudinal spring and summer of 5 m would result in 0.25 K month^{-1} δ(SST) change (with $\delta(\eta = -\overline{h}_{\mathrm{mix}}^{-2}\delta(h_{\mathrm{mix}})$ a monthly mean $\overline{h}_{\mathrm{mix}}$ = 50 m, $\overline{F}$ = 200 W m^{-2}, c_p = 4000 J kg^{-1} K^{-1} and ρ = 1026 kg m^{-3}). This monthly change of SST is well within its observational accuracy on a global basis [*Reynolds and Smith*, 1994]. The closure of *Alexander et al.* [2000] is the importance of anomalous h_{mix}, beside heat flux variations, during spring and summer north of 20°N.

[5] The impact of anomalous entrainment out of the mixed layer base to the SST tendency is indirectly through h_{mix}. The stored anomaly of thermal energy beneath the seasonal thermocline can last for many years, which in our context is represented by the third term on the right hand side of equation (1). Thermal anomalies of the previous winter become entrained into the current winter mixed layer as the mixed layer deepens in the fall [*Alexander et al.*, 2000]. The implementation of this "reemergence mechanism" could also directly extend the persistence of winter SST anomalies to several years [*Alexander and Deser*, 1995; *Deser et al.*, 2003]. Therefore, to quantify, understand and ultimately predict ocean-atmosphere interactions on seasonal-to-climate relevant timescales it is crucial that the sensitivity of anomalous SST to changes of h_{mix} be well modeled in comparison to observations.

[6] A more complicated set of processes, as wind stress changes that force horizontal currents to advect thermal energy from place to place seem to explain a portion of the observed SST changes in the El Niño–Southern Oscillation (ENSO) regime in the tropical Pacific [*Jin*, 1997]. Additional changes are caused by the mixed layer depth anomalies, including turbulent fluxes out of the mixed layer bottom [e.g., *Wang and McPhaden*, 2001], internal waves, and ocean eddies. To be useful in climate analyses and climate modeling, the uncertainty of the h_{mix} must match the uncertainty of SST observations, or in our context, that all terms in equation (1) have comparable errors. The two major reasons for the lack of observed h_{mix} are the insufficient number of observations, both in spatial and temporal senses, to average the effects of internal waves and ocean mesoscale [e.g., *Moisan and Niiler*, 1998] and that h_{mix} is not a directly measurable quantity. The ocean mixed layer depth h_{mix} is most commonly defined as that depth where the temperature (potential density) has decreased (increased) from the surface value by a constant amount Δ. For climatological profiles on a global scale it is found that the Δ criterion introduces an error of 20 m in h_{mix} [*Kara et al.*, 2000b], which is several times larger than the error of the terms in equation (1) introduced by SST or flux errors. The error in h_{mix} seems to be reduced when applying the threshold method to individual profiles [*de Boyer Montégut et al.*, 2004].

[7] The main focus in this paper is to establish a new criterion for h_{mix} that can be used globally to study the large-scale processes of thermal energy storage in the upper ocean in both observations and in OGCM simulations. In this respect h_{mix} should be considered in a similar way that the high-quality SST is currently used for a diagnostic of the upper ocean processes. We require from the introduced criterion that it minimizes systematic errors between estimates of h_{mix} based on measured data and the output of OGCMs and that applications of the criterion to both data sets provide comparable statistics for h_{mix}, respectively. This analysis should make model-data comparison more stringent because not only must SST be correct, but also its first vertical moment, or h_{mix}. We use the global historical hydrographic measurements with both high and low vertical resolutions, including the World Ocean Circulation Experiment (WOCE) data set, and a full OGCM output to determine whether calculations of h_{mix} and its variability can be improved.

[8] The paper is organized as follows: In section 2 we present the data and discuss the difficulties in estimating h_{mix} from these data; we then introduce a new criterion for estimating an h_{mix} (which we refer to as $h_{\mathrm{mix}/c}$) and test the sensitivity of $h_{\mathrm{mix}/c}$ to the assumptions made in our new criterion and also compare our results with the more traditional Δ criterion. In section 3 we introduce a "quality index" and discuss the quality of the observed $h_{\mathrm{mix}/c}$. In section 4 we describe some characteristics of $h_{\mathrm{mix}/c}$ and its space and time variability over ocean basins. In section 5 we apply our algorithm for h_{mix} to the output of the Massachusetts Institute of Technology (MIT)/OGCM/Estimating the Circulation and Climate of the Ocean (ECCO) model in an assimilation mode and compare $h_{\mathrm{mix}/c}$ to the diagnosed planetary boundary layer depth in the model *K*PP parameterization. A summary of our results is given in section 6.

2. Problems of Estimating Mixed Layer Depths

2.1. Data Set

[9] We use the quality controlled hydrographic global measurements from mechanical bathythermographs (MBTs), expendable bathythermographs (XBTs) and conductivity-temperature-depths (CTDs) with high and low vertical resolution (the depth interval is equal to 1–5 m and 20 m, respectively). These are filed by *World Ocean Circulation Experiment International Project Office, WOCE Data Products Committee* (*WOCE IPO*) [2002] (and available at http://www.nodc.noaa.gov/woce_v3). The MBT temperature measurements provide the longest (from the early 1950s until the mid-1990s) and the most extensive time series (2.4 million profiles). The vertical resolution of these profiles is irregular and most of the profiles do not extend below 200 m (maximum depth is around 700 m). Almost the same number (about 2.1 million) of temperature profiles from XBTs is available, some of which reach depths of 700–1500 m with an interval of 2 m. However, the XBT data show quite often a gap between the surface value ($\sim$0 m) and the second measuring point (about 10–30 m); this includes a temperature jump of $\Delta T \sim 0.2$ K which

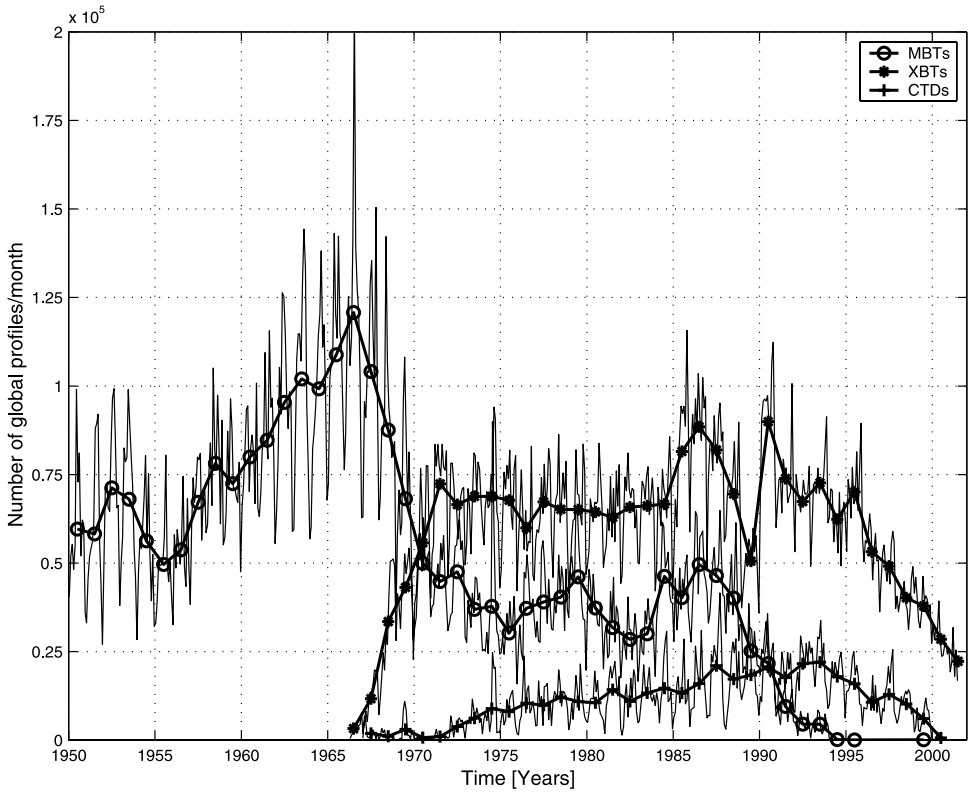

Figure 1. Number of global high- (1–5 m) and low- (20 m) resolution profiles provided by *WOCE IPO* [2002] (also available at http://www.nodc.noaa.gov/woce_v3): MBT, XBT, and CTD measurements are marked by circles, asterisks, and pluses, respectively. Annual and monthly means are indicated by heavy and thin solid lines, respectively.

effects the estimation of h_{mix} using a small ($\Delta T \leq 0.2°\mathrm{C}$) threshold criterion. Therefore we start the estimation method of h_{mix} at the second measuring point to avoid artificial mixed layer depth between the first two measuring points. The CTD temperature and salinity profiles (0.4 million) typically extend over the whole water column with a spacing of 1–2 m. XBT and CTD profiles become readily available after the late 1960s (Figure 1).

[10] We also use the daily temperature profiles from the Tropical-Atmosphere-Ocean(TAO)/Trition (T/T) buoy array (http://www.pmel.noaa.gov/tao). The first buoys were deployed along 110°W in late 1984. The array currently consists of approximately 70 deep ocean moorings (from the surface down to 500 m) with 2°–3° meridional and 10°–15° zonal resolutions, spanning an area between 8°S and 8°N, 137°E and 95°W. To be consistent with our ECCO model-data comparison, we chose the time frame from 1992 to 2001 that covers both the 1992–1995 and 1997–1998 El Niño cycles [*Wang and McPhaden*, 2001]. Since these data are not continuously distributed in space and time, we normalized monthly means by the number of days of data per month. For our study, data are available from 7 depth levels, at 20 m separation to 140 m, and SST is the temperature at 1 m depth.

[11] The model data comes from a 1° × 1° 1992–2001, global adjoint run of the ECCO model where the daily average temperature is used to diagnose h_{mix}, using both the Δ criterion as well the criterion introduced below for computing h_{mix} (namely, A. Köhl et al., The ECCO 1 degree global WOCE Synthesis, ECCO Report 20, Nov. 2002, available at http://www.ecco-group.org/reports.html). Daily average ocean planetary boundary layer depths h_{pbl} that are the depths to which surface-forced turbulent mixing penetrates in the "*K* profile parameterization" (*K*PP) are also retrieved from the model solution.

2.2. Definitions for the Ocean Mixed Layer Depth h_{mix}

2.2.1. The Δ Criterion and Its Limitations

[12] Direct measures of turbulence in the near sea surface layer or turbulent dissipation rates [*Brainerd and Gregg*, 1995] are rare, so the actively turbulent layer cannot be defined on basin scales by direct turbulence observations. Overturning scales of 10 cm could potentially be used, but the very high resolution profile data are not filed in the public data sets. The "mixed layer" in our coarse (>2 m) vertical resolution data is the zone of relatively homogeneous water formed by the history of turbulent mixing, including zones where water masses created by deep convection, "mode waters" [*Talley and Raymer*, 1982], abound. We endeavor to find the homogeneous layer closest to the surface, believing that we have captured the effect of the most recent, above the daily cycle, mixing events. The simplest concept is to define the ocean mixed layer depth h_{mix} as the depth where the quasi-homogeneous profile of temperature has decreased (potential density increased) from a "reference" value, most commonly the surface value, by a constant amount, Δ (various published Δ criteria are listed by *Kara et al.* [2000b] and *de Boyer Montégut et*

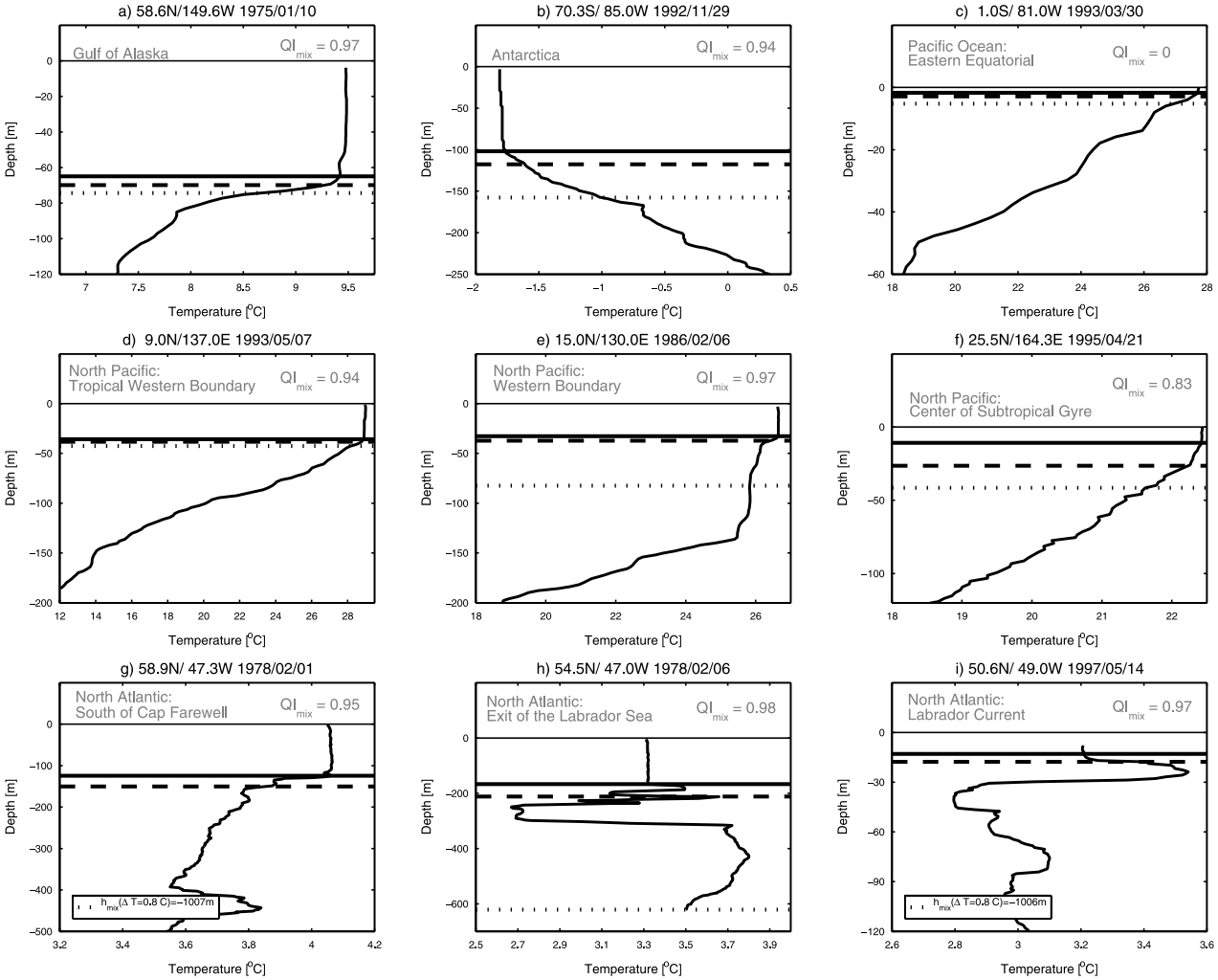

Figure 2. Variety of high-resolution CTD temperature profiles. The ocean mixed layer depth h_{mix} (defined by two types of Δ criteria ($\Delta T = 0.2^{\circ}$C and $\Delta T = 0.8^{\circ}$C) and the criterion of the present study) is indicated by dashed, dotted, and solid lines, respectively. (The quality index $\mathrm{QI}_{\mathrm{mix}}$ of the ocean mixed layer is defined in section 3.4).

al. [2004]). According to *Lukas and Lindstrom* [1991], a potential density based Δ criterion is more reliable than the temperature based, because in many regions the temperature profile does not capture the vertical stratification correctly. However, density profiles show significant areas where h_{mix} is determined by a halocline. ''Barrier layer'' regions [*Sprintall and Tomczak*, 1992] are identified by a deeper temperature-based h_{mix} than the density-based h_{mix}; the latter h_{mix} is deeper than h_{mix} based on temperature profiles in ''vertically density-compensated areas'' [*de Boyer Montégut et al.*, 2004, paragraph 1]. Presently, the available density profiles are about an order of magnitude less than the temperature profiles (e.g., Figure 1). For most parts of this paper we use temperature profiles, unless explicitly indicated. In section 3.1 we address some of the differences that result in h_{mix} computations when using the density profiles.

[13] We can see from the variety of temperature profiles, which features the complexity of the upper ocean vertical structure (Figure 2) that the stratification depends strongly on the dynamical regions and the seasons. Thus a value of Δ chosen subjectively for one region or season might not be applicable to another region or season. Even if a profile shows a well-defined mixed layer and the ΔT is within the observed temperature range, the depth of the mixed layer is not defined accurately by the Δ criterion (Figures 2b, 2f, and 2h). *Kara et al.* [2000b] computed h_{mix} from both monthly climatological data of the ocean weather station P in the northeast Pacific and the Levitus climatology [*Levitus et al.*, 1994; *Levitus and Boyer*, 1994]. *Kara et al.* [2000b, p. 16,803] concluded ''that the inherent variability of h_{mix} only allows for an accuracy of 20 m in 85% of the cases'' (using a 0.8°C criterion). Deriving at h_{mix} from in situ profiles, recently, *de Boyer Montégut et al.* [2004] showed that a threshold of 0.2°C is most appropriate to result in optimal estimates of h_{mix}. Systematic biases of h_{mix} develop when the Δ criterion is applied to idealized temperature profiles that are demonstrated in detail on Figure 3.

[14] The Δ criterion depth h_{mix} is sensitive to the following.

[15] 1. For the chosen Δ (Figure 3a), the larger Δ, the deeper is h_{mix} (blue lines). Note in particular that this bias is

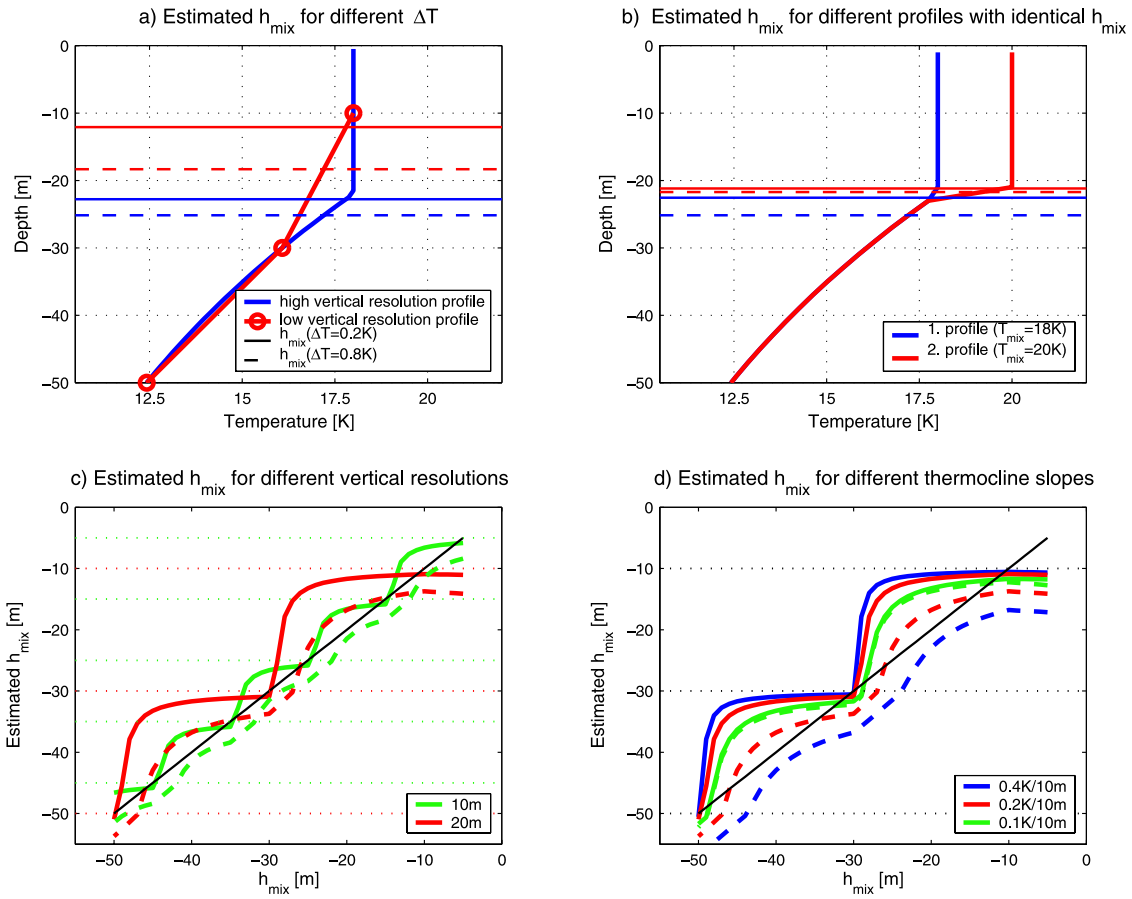

Figure 3. Systematic errors of h_{mix} based on the Δ criterion: Idealized high- (2 m) and low- (20 m) resolution temperature profiles. Corresponding estimated h_{mix} for (a) two different ΔT and (b) two different profiles (simulated with different temperatures of h_{mix} but identical h_{mix}). (c) Sensitivity of h_{mix} to the vertical resolution, whereby the vertical gradient at the base of the mixed layer matches 0.2 K $(10\ \mathrm{m})^{-1}$ for Figures 3a–3c. (d) Sensitivity of h_{mix} to the vertical gradient at the base of the mixed layer (with a vertical resolution of 20 m), whereby the red lines in Figure 3d correspond to the red lines in Figure 3c. For Figures 3a–3d, estimates of h_{mix} with $\Delta T = 0.2°\mathrm{C}$ and $\Delta T = 0.8°\mathrm{C}$ are indicated by solid and dashed lines, respectively.

not negligible when small vertical gradients at the base of the mixed layer occur.

[16] 2. For the "reference value" (Figure 3b), the smaller the difference between the temperature of the mixed layer (the reference value) and the one below and the smaller the vertical gradient at the base of the mixed layer, respectively, the larger is h_{mix}. This implies an artificial dependence of h_{mix} on the reference value, or SST.

[17] 3. For the vertical resolution (Figure 3c), linear interpolation in low vertical resolution profiles leads to a smaller value, or shallow bias of h_{mix}. In other words, the lower the vertical resolution, the larger the tendency of h_{mix} to cluster at the levels where the data is sampled and sampling levels become "sticking points" for h_{mix} (see also red lines in Figure 3a).

[18] 4. For the vertical gradient at the base of the mixed layer (especially in the 20-m resolution case) (Figure 3d), the larger the vertical gradient at the base of the mixed layer the smaller (by about 20%) and the "stickier" is h_{mix}.

[19] The tendency of h_{mix} to cluster at sampling levels seems to be enhanced for small Δ applied to low-resolution profiles and then relatively independent from the stratification below h_{mix}. In the 20-m resolution case, with a vertical gradient at the base of the mixed layer of 0.2 K $(10\ \mathrm{m})^{-1}$, h_{mix} estimated for $\Delta T = 0.2°\mathrm{C}(\Delta T = 0.8°\mathrm{C})$ shows an offset from the ideal h_{mix} by 5 m(4 m); with a vertical gradient of 0.1 K $(10\ \mathrm{m})^{-1}$ the standard deviation yields 4 m(2 m).

[20] In summary, the above discussion points to three major concerns about the Δ criterion method. First, if we assume that a $\Delta T = 0.2°\mathrm{C}$ is representative of an adequate criterion for the threshold method [*de Boyer Montégut et al.*, 2004], the estimated h_{mix} is often below the visible point in the profile that clearly marks h_{mix} (Figures 2b, 2f, 2g, and 2h); the resulting deviations can be sometimes in the order of h_{mix} itself (Figure 2f). Second, the complicated dependence of h_{mix} on the vertical resolution is not desirable, especially when comparison studies are made with the low vertical resolution output of OGCMs. Third, because h_{mix} depends on the SST or a reference value and there is no rational choice for this value leads us to be a more than skeptical that the turbulent region of the upper ocean is captured well by the Δ criterion. We are thus motivated to

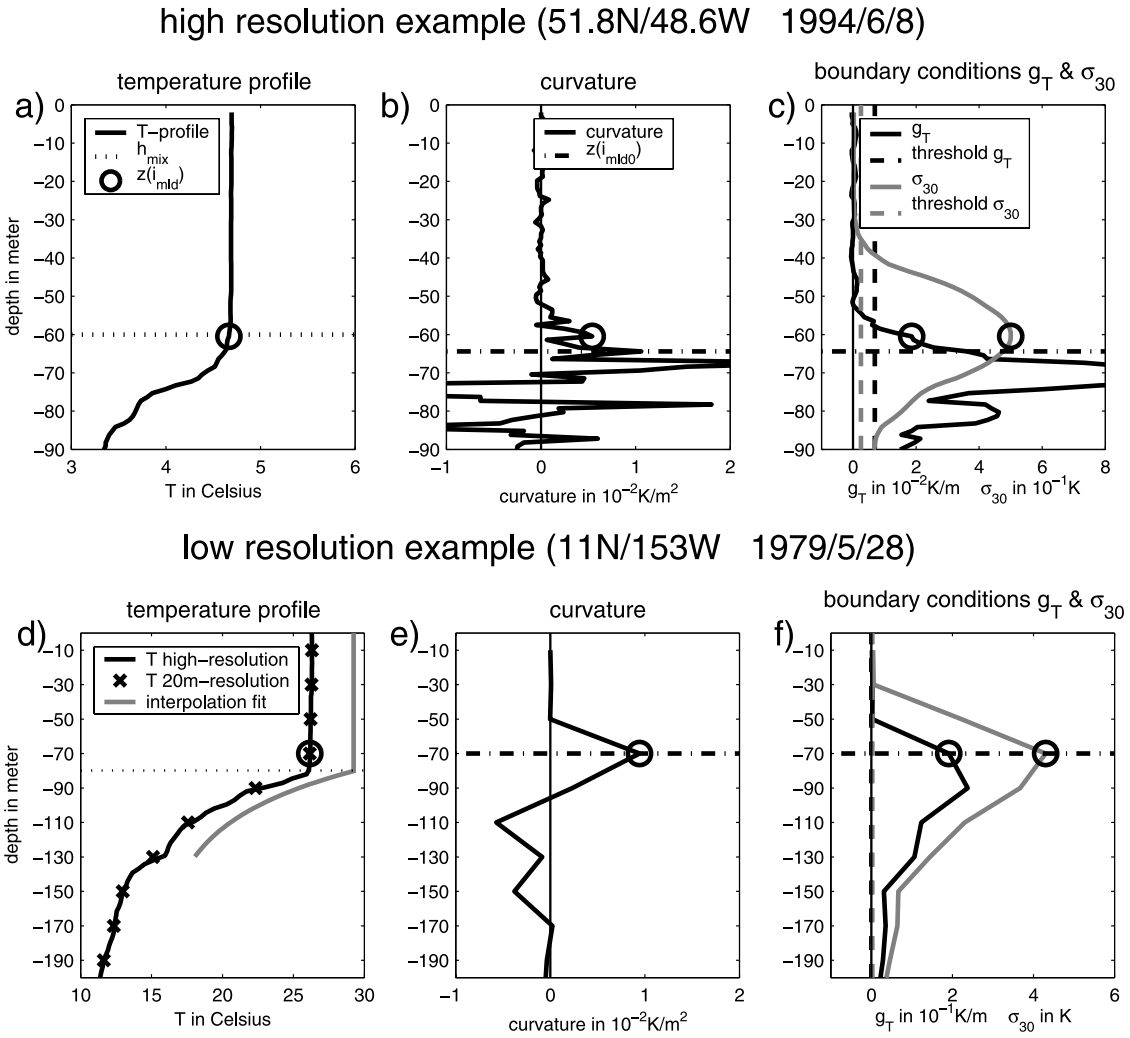

Figure 4. (a–c) High and (d–f) low vertical resolution temperature profile considered as example to illustrate the h_{mix} estimation. The legends should go along with the word description of our concept estimating h_{mix} in section 2.2.2. The black open cycle marks the level closest to h_{mix}, $z_{i_{\mathrm{mld}}}$ (namely, section 2.2.2). The (exponential) interpolation fit (grey solid line in Figure 4d)) is shifted by 3°C for better comparison.

seek a more universal criterion that can be applied to computing mixed layer depths.

2.2.2. Gradient Method and Our Method, a Curvature-Based Criterion

[21] Consider now the information that can be gleaned from inspection of temperature gradients. *Large et al.* [1986] suggested using the vertical gradient where h_{mix} is taken to be the shallowest depth where the vertical density gradient is equal to twice the average gradient from the surface to 120-m depth. Since the temperature profiles are often smoothed to 5-m resolution further choice has to be made on how to smooth the salinity spikes or the length scale over which the gradients are computed. Like the Δ criterion, the gradient criterion depends critically on the prescribed gradient threshold; in addition, the threshold is usually kept constant for all space and time (see listing by *Kara et al.* [2000b]). In comparison with the Δ criterion the vertical gradient-based criterion seems also to be less robust [*Brainerd and Gregg*, 1995]. Besides the threshold methods (and in absence from direct turbulent measurements), h_{mix} is derived from oceanic profiles, by less conventional methods, like the "integral," "least squares regression," and "split-and-merge" methods (taken up and recently introduced, respectively, by *Thomson and Fine* [2003]).

[22] The above considerations led us to look for a method that does not depend critically upon the choice of values of a number of parameters which are to take the best compromise to deal with the global ocean. Consider, hence, the information contained in the second derivative, or "curvature," of the profile. Perhaps the first local extreme value of the curvature of temperature or density profile is a distinguishing feature of the depth to which the most recent mixing events penetrate. An advantage of this approach is that, unlike threshold methods, the estimated h_{mix} is not a linear function of another dynamical quantity, such as the SST for instance and is less dependant on the dynamical region or seasons, respectively. First of all our approach

specifies an interval in depth where h_{mix} should be identified which requires the choice of mainly two parameters as boundary conditions. Afterward the approach searches within this interval after the first extreme curvature of the profile and interpolates from its depth to h_{mix}. The detailed description of our approach follows below; Figure 4 accompanies the description considering as example a high- and low-resolution temperature profile. The complete MATLAB code is listed in the auxiliary material[1].

2.2.2.1. Defining Derived Quantities

[23] We define the depth $z(i)$ as negative definite and refer to $i = 1$ as the level closest to the surface. Gradients of the vertical profiles at level i are defined as

$$g_T(i) = \frac{T(i) - T(i_{5\,m})}{z(i) - z(i_{5\,m})}, \tag{2}$$

where the index $i_{5\,m}$ refers to the next deeper level, which is at least 5 m deeper than the level i, for a smoother and more stable estimate of g_T. Note, since we are interested in $g_T(i)$ only as a boundary condition for the estimation of the level closest to h_{mix} we defined the gradient $g_T(i)$ as the gradient below the level i and not as the centered gradient; g_T is positive if T decreases with depth (see Figures 4c and 4f). The curvature is

$$c_T(i) = \frac{g_T(i) - g_T(i-1)}{z(i-1) - z(i)}; \tag{3}$$

$c_T(i)$ is centered, and it is positive if g_T above the current level is smaller than g_T of the current level (see Figures 4b and 4e).

[24] As a second boundary condition for the estimation of the level closest to h_{mix} we evaluate the variability of the profile in a 30-m region below the current level, in order to distinguish a near homogeneous region from a region of rapid change. We define $\sigma_{30}(i)$ as the standard deviation of T over the levels in a 30-m interval below the current level (the current level included) (see Figures 4c and 4f).

2.2.2.2. Truncation Condition

[25] If $\max[\sigma_{30}] < 0.02$ K we set $h_{mix} = \min[z]$. Hence, if no region of significant inhomogeneity exist in the profile, then h_{mix} must be below the lowest measured level (these profiles are flagged in the computing algorithm).

2.2.2.3. A First Guess of h_{mix}

[26] We define a lower limit in the profile, $z(i_{mld0})$, in which the h_{mix} can be found; $z(i_{mld0})$ is the first level with $|g_T(i)| > 0.25 \max[g_T]$ and $\sigma_{30}(i) > 0.02$ K. This level usually refers to the top of the thermocline and is closely below h_{mix} (see Figures 4b and 4c). This range is used to estimate the scale of a significant gradient, σ_{g_T}, which is defined as the standard deviation of g_T over the interval $[z(1), z(i_{mld0})]$, similar to the gradient based approach of *Large et al.* [1986]. Additionally, we set the absolute lower limit for σ_{g_T} to 0.004 km^{-1} for high (<6 m) and 0.002 km^{-1} for low vertical resolution profiles, respectively (finite difference measurement errors in the gradient estimation match the half of these empirical values).

2.2.2.4. Level Closest to h_{mix}

[27] The level closest to h_{mix}, $z(i_{mld})$, is the first local maximum/minimum of c_T that falls together with a positive/negative gradient g_T. Additionally we ask for two boundary conditions: First, $|g_T| > \sigma_{g_T}$, which defines a threshold for a significant local inhomogeneity in the profile. As a second boundary condition we demand that $\sigma_{30} > 0.02$ K. This second condition takes a more global point of view. It assures that $z(i_{mld})$ refers to a point above a region of rapid changes and not just a small-scale intrusion, which is important for high-resolution profiles ($z(i_{mld})$ is marked throughout Figure 4).

[28] If no extreme value is found in this upper subsection of the profile, we set $z(i_{mld})$ to the first level with $g_T \geq 0.7$ max $[g_T]$. This condition happens for typically shallow mixed layers. Less than 1% of the profiles are affected if h_{mix} exceeds 40 m.

2.2.2.5. Interpolation

[29] For low-resolution data it is important to interpolate h_{mix} between the levels, in the interval $[z(i_{mld} - 1), z(i_{mld} + 1)]$. Our interpolation scheme essentially assumes that the profile follows the idealized structure illustrated in Figure 3. Therefore we fit an exponential function $fit(z) = C + Ae^{Bz}$ to the interval $[z(i_{mld}), z(i_{mld} + 2)]$ if possible; that means $A, B, C \in R$ and $B > 0$. h_{mix} is defined as the depth z for which $fit(z) = T_{mix}$, where T_{mix} is the mean temperature in the interval $[z(1), z(i_{mld})]$. Hence h_{mix} is interpolated in the interval $[z(i_{mld} - 1), z(i_{mld})]$. However, in cases where $g_T(i_{mld} - 1)$ is both less than 10% of $g_T(i_{mld})$ and an exponential fit is possible from $z(i_{mld} + 1)$, we shift the interpolation into the interval $[z(i_{mld}), z(i_{mld} + 1)]$ (see example in Figures 4d–4f). Note that such an exponential interpolation my also improve the h_{mix} estimate of a Δ criterion based method.

[30] If an exponential fit is not possible we use a simple linear function for $fit(z)$ with the gradient $((g_T(i_{mld} - 1) + g_T(i_{mld}))/2)$ and use $T_{mix} = T(i_{mld} - 1)$ as reference. If both an exponential fit is not possible and $|g_T(i_{mld} - 1)| < |g_T(i_{mld})|$, the profile does not fit to the idealized structure illustrated in Figure 3. We then use a simple linear interpolation to the reference value $T_{mix} = T(i_{mld} - 1) \pm \delta T$, where δT is the maximum T difference between two consecutive levels found in the interval $[z(1), z(i_{mld} - 1)]$.

[31] For high-resolution (<6 m) profiles we always use the linear interpolation. In order to optimize our interpolation scheme we compared the estimated h_{mix} based on high-resolution profiles to the estimated h_{mix} based on the same profiles but with reduced 20-m resolution, assuming that the high-resolution estimate is the "real" h_{mix}. The examination of many observed low-resolution CTD profiles revealed that both the exponential and the linear fit have a small systematic offset to the real h_{mix}, which we empirically corrected with an additional small linear shift.

[32] Note that our method is an empirical method based on the visual examination of high-resolution (~2 m) temperature profiles of the entire global WOCE-CTD data set, a copy of it which was artificially reduced to 20-m resolution profiles and data from a numerical MIT-OGCM integration. The crucial parameters for this method are the boundary conditions for the first local maximum/minimum of c_T (section 2.2.2.4). These parameters essentially define the level of inhomogeneity in the profile, which we consider as

[1] Auxiliary material is available at ftp://ftp.agu.org/apend/jc/2003jc002157.

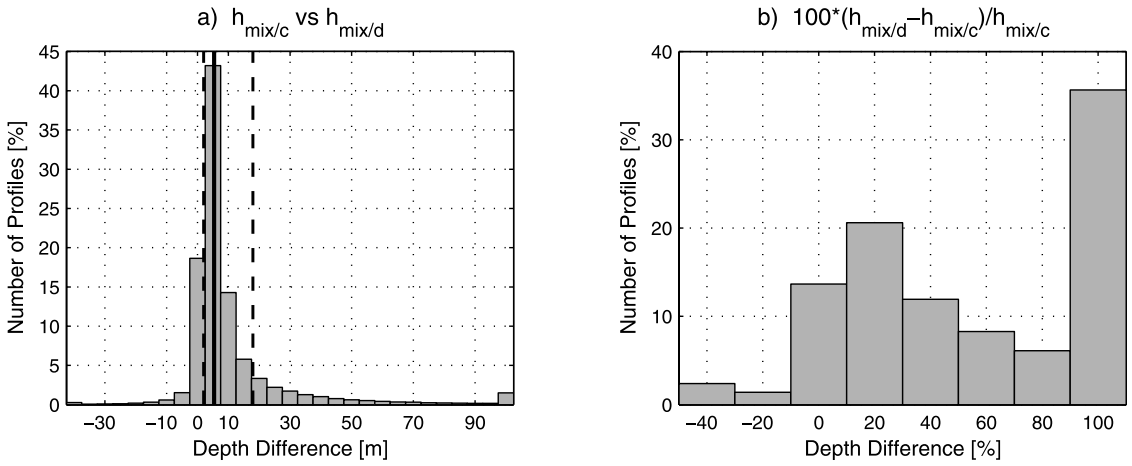

Figure 5. (a) Histogram of differences between $h_{\mathrm{mix}/d}$ (ΔT = 0.2°C) and $h_{\mathrm{mix}/c}$ inferred from high-resolution CTD-temperature profiles in which the black solid line marks the median (depth bins, 5 m), and the black dashed lines mark the 70% interval around the median, respectively. (b) Same as Figure 5a but for relative difference. Valid in both cases: negative, deeper $h_{\mathrm{mix}/c}$.

indications for h_{mix}. Note that unlike a Δ criterion the $h_{\mathrm{mix}/c}$ is not a direct function of these parameters and, in turn, these parameters are not a direct function of another physical quantity (such as SST). Therefore small variations of the parameters will not lead to proportional changes in $h_{\mathrm{mix}/c}$, which is one of the advantages of our method. Additional parameters (section 2.2.2.3) refer to the measurement uncertainties. For high-resolution data, the smoothing of the gradients assures that small-scale intrusions do not effect the estimation of $h_{\mathrm{mix}/c}$. We especial took a careful examination of critical regions/seasons such as the winter time deep convection regions in the northern North Atlantic as well as the tropical regions with a rather smooth transition into the thermocline. The parameters we use are empirically chosen, and were optimized to some degree by variations of a single parameter and a visual examination of all profiles for which the h_{mix} estimate was changed.

[33] To apply the above criterion to salinity or potential density profiles, we multiply the parameters by 10 and 4, respectively, since the ratio of the standard deviation of salinity/potential density in the upper 500 m to the one of temperature tend to correspond to 0.1/0.25.

2.3. Comparison of $h_{\mathrm{mix}/c}$ With the Δ Criterion

[34] A number of significant differences were found between $h_{\mathrm{mix}/c}$ and $h_{\mathrm{mix}/d}$, at which the latter uses the 0.2°C criterion following *de Boyer Montégut et al.* [2004]. The histogram of differences between $h_{\mathrm{mix}/c}$ and $h_{\mathrm{mix}/d}$ was computed from the entire ensemble of CTD-temperature profiles (Figure 5a). The difference is skewed toward larger $h_{\mathrm{mix}/d}$ and is not a Gaussian distribution. The mainly positive outliers indicate that $h_{\mathrm{mix}/d}$ is systematically larger than $h_{\mathrm{mix}/c}$ by 6 m. The 70% interval around the median of the differences is 2–18 m. The differences between $h_{\mathrm{mix}/c}$ and $h_{\mathrm{mix}/d}$ are much larger than one may have expected assuming that observed profiles are just noisy versions of the profiles in Figure 3 and therefore $h_{\mathrm{mix}/d}$ is just systematically shifted deeper due to its finite Δ value. However, the visual inspection of the examples in Figures 2b, 2i, 2f, and 2h, already indicated that larger differences between $h_{\mathrm{mix}/c}$ and $h_{\mathrm{mix}/d}$ exist, which are due to the complex nature of the profiles. We randomly chose 500 profiles where the relative differences were more than 20% and a visual inspection for these profiles, like the one used in Figure 2, showed that in 63%, $h_{\mathrm{mix}/c}$ appeared to render a more realistic value for upper ocean homogeneous depth than did $h_{\mathrm{mix}/d}$, whereby in 10% $h_{\mathrm{mix}/d}$ looked to be more reliable. For the remaining 27% it is not definite which one of the two criteria reproduces the adequate h_{mix} (see Figures 2a, 2d, and 2e).

[35] Since smaller differences at small $h_{\mathrm{mix}/c}$ appear to be more significant for the upper ocean heat budget than at larger values we relate the difference between $h_{\mathrm{mix}/c}$ and

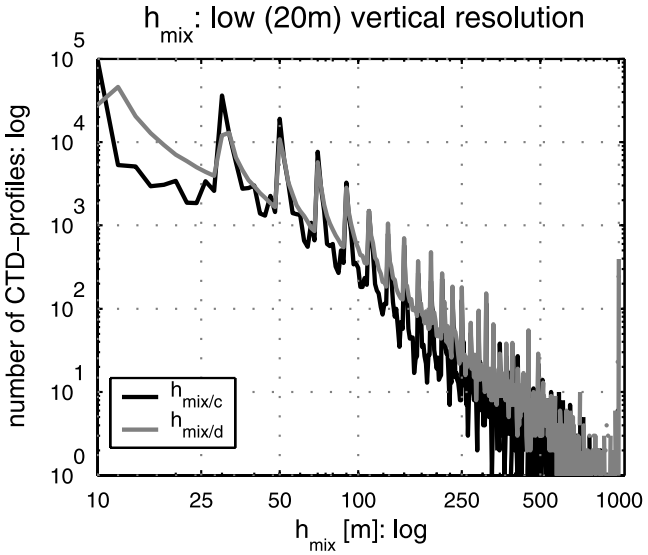

Figure 6. Distribution of h_{mix} inferred from low- (20 m) resolution CTD-temperature profiles; $h_{\mathrm{mix}/c}$ and $h_{\mathrm{mix}/d}$ (ΔT = 0.2°C) is indicated by a black and gray lines, respectively (depth bins, 2 m). Analyses for σ_Θ show a similar behavior.

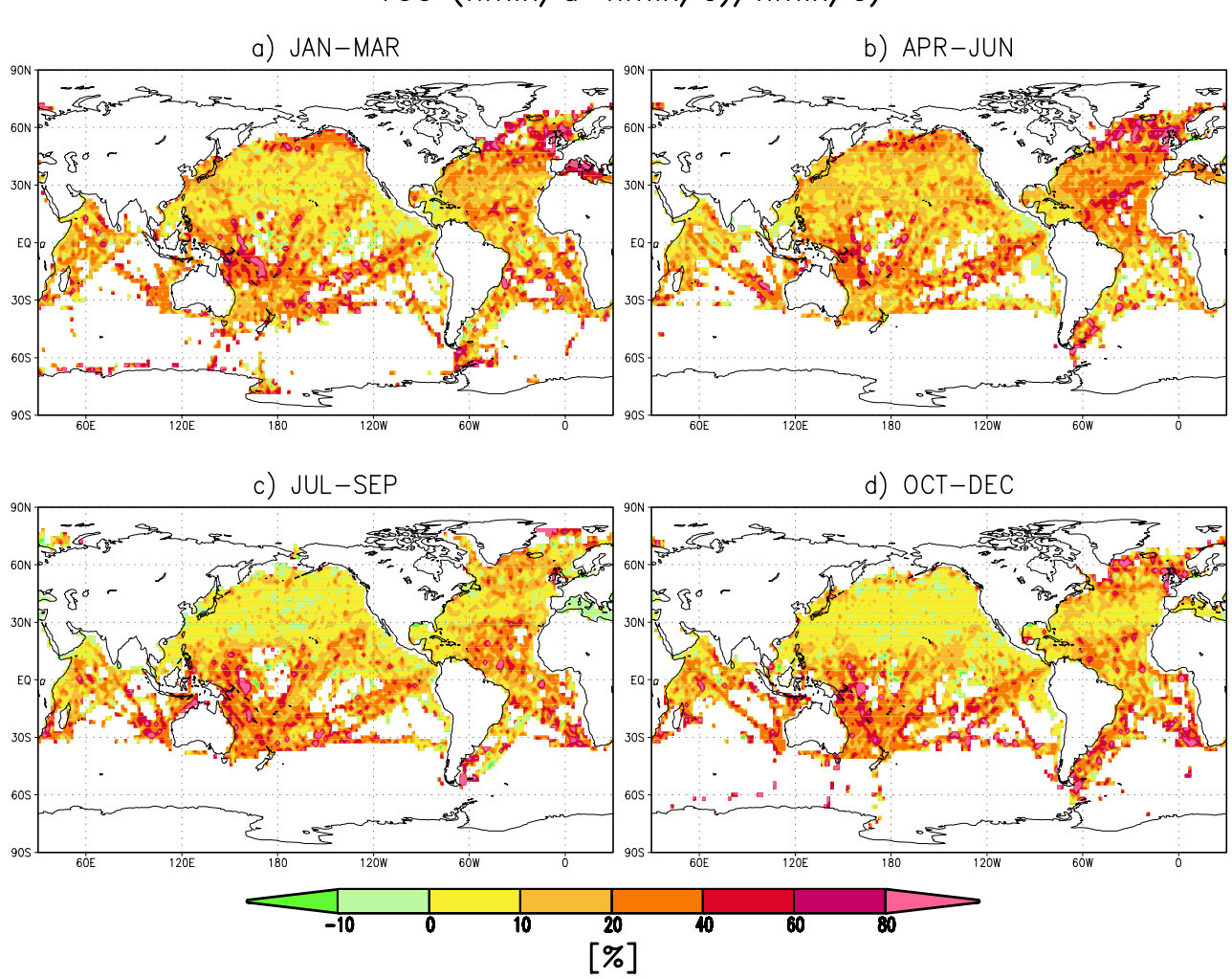

Figure 7. Relative difference (in percentage) between long-term monthly mean $h_{mix/d}$ ($\Delta T = 0.2°C$) and $h_{mix/c}$ inferred from temperature profiles of the combined CTD-XBT data set of Figure 1 (negative, deeper $h_{mix/c}$; white, undefined values).

$h_{mix/d}$ to the magnitude of $h_{mix/c}$ (Figure 5b). The general conclusion is the same as for the nonnormalized differences that about one third of all $h_{mix/d}$ are more than 100% larger than $h_{mix/c}$. The relative difference peaks at 20% (Figure 5b). (For the occurrence of a relative difference of h_{mix} above 100% we refer to Figures 2c and 2f.) The curvature criterion finds small values of mixed layers what the Δ criterion does not. For instance focus on $h_{mix/c}$ in the Northern Hemisphere: When $h_{mix/c}$ is smaller or equal 10 m and/or is in the first half of the year, most of the relative differences exceed the 100% value. When $h_{mix/c}$ is deeper and/or is in the second half of the year the differences that exceed 100% are reduced to one fourth and the remaining distribution of the relative difference peaks at around 20% (not shown).

[36] The distribution of h_{mix} stays flat until h_{mix} reaches 50 m; for deeper h_{mix} it decays rapidly with increasing h_{mix} (Figure 6); these shape functions are independent of the method used. In addition the curve progression of h_{mix} shows clearly the overestimation of h_{mix} by the Δ criterion if h_{mix} exceeds 50 m.

[37] To have a better global and temporal coverage, we combine CTD data with XBT data (see Figure 1). In the Northern Hemisphere, spatial pattern of the relative difference between the long-term seasonal mean $h_{mix/c}$ and $h_{mix/d}$ shows some zonal structures (Figures 7a–7d) that reflect the effects of the progression of the seasonal thermocline on the $h_{mix/d}$ computation. In the thermodynamically active cooling regions in winter and spring, poleward of 40°N, the relative differences exceed 20% (Figures 7a–7d) as predicted by comments in the discussion of Figure 5b. A global uniform ΔT of 0.2°C is often too large to capture the small vertical gradients and is often too close to the observed temperature range to be useful. Therefore $h_{mix/d}$ is generally deeper than $h_{mix/c}$ (Figures 7a and 7b). In the midlatitude North Pacific the top of the main thermocline stratification is strong enough that the overestimation of $h_{mix/d}$ is below 20% (Figures 7a and 7b).

[38] The relative difference of h_{mix} is reduced in both the midlatitude North Pacific and North Atlantic during summer and fall due to the existence of a distinctive seasonal thermocline (Figures 7c and 7d). The seasonal thermocline

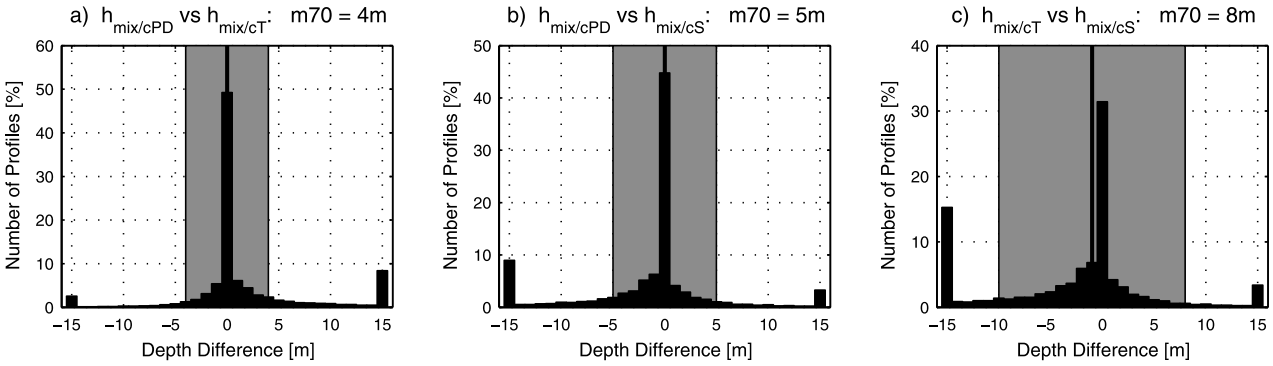

Figure 8. Histogram of differences between $h_{\mathrm{mix}/c}$ estimated for (a) temperature (T), (b) salinity (S), and (c) potential density (PD) profiles based on CTD data (depth bins, 1 m). Shaded areas mark the 70% interval around the median, the interval of the "m70" value (negative, first labeled $h_{\mathrm{mix}/c}$ in the title deeper).

is much better developed in the western portion of each gyre than in the eastern portion [e.g., *Tomczak and Godfrey*, 1994].

[39] The relative difference of h_{mix} using a larger threshold ($\Delta T = 0.8°\mathrm{C}$) is much more pronounced even if the main characteristics are similar to the difference using the 0.2°C criterion. One discrepancy is that the relative difference shows a zonal gradient in the midlatitude North Pacific (not shown). Therefore the 0.8°C criterion seems not to be able to capture the observed temperature range between the seasonal and permanent thermocline in the eastern midlatitudinal North Pacific as it does in the western; whereby the 0.2°C criterion does take into account the effects of the seasonal thermocline and we find that the relative difference is less than 10% (Figures 7c and 7d). This supports the finding from *de Boyer Montégut et al.* [2004] that the 0.2°C criterion is more successful following the seasonal variability of h_{mix} than a more commonly used larger Δ criterion.

[40] In the tropics around ±20° latitude of the equator the near surface stratification is characterized by a weak seasonal cycle. In this band a definition of a seasonal cycle of stratification in the upper 50–100 m is not well established since the daily cycle of turbulent mixing is typically stronger than seasonal-to-interannual changes. However, $h_{\mathrm{mix}/d}$ appears to be in generally larger by about 20% than $h_{\mathrm{mix}/c}$. The water column is weakly stratified just below the surface and the profiles of temperature within the top of the main thermocline are concave. The vertical gradients differ weak until the top of the thermocline is reached (see section 2.2.2), so a smaller h_{mix} is found in these regions of positively curved profiles by searching for the location of the extreme curvature than the Δ criterion. In the southwestern equatorial Pacific the relative difference between $h_{\mathrm{mix}/d}$ and $h_{\mathrm{mix}/c}$ is larger than 40% throughout the year. Under "normal" (light) wind conditions this region is weakly stratified in temperature until the top of the thermocline; a threshold criterion captures the depth of the top of the thermocline including a barrier layer and overestimates the depth of the well-mixed region, respectively, except during west wind bursts when barrier layers disappear. The sensitivity of the curvature criterion to small-scale inhomogeneities in the temperature profile at the top of a barrier layer explains shallower $h_{\mathrm{mix}/c}$ than $h_{\mathrm{mix}/d}$. Studies of *Lukas and Lindstrom* [1991] seem to confirm the result of a mixed layer that is shallower than previous estimates; their threshold method found nearly isothermal layers that are deeper by about 33% than the real mixed layers as estimated with density profiles. Further comparisons between $h_{\mathrm{mix}/c}$ and $h_{\mathrm{mix}/d}$ are taken up in sections 3.2 and 4.

3. Effects of Salinity, Vertical Resolution, and a Quality Index for h_{mix}

3.1. Effects of Salinity

[41] Potential density profiles are computed from the CTD profiles of temperature and salinity. The buoyancy of the upper ocean water column is in a condition where thermal gradients account for 67% of the density variability and salinity for 33% [*Speer et al.*, 1995]. The differences between $h_{\mathrm{mix}/c}$ inferred from profiles of temperature ($h_{\mathrm{mix}/cT}$), salinity ($h_{\mathrm{mix}/cS}$) and potential density ($h_{\mathrm{mix}/cPD}$) show (Figure 8) that in 70% of the cases $h_{\mathrm{mix}/cT}$ and $h_{\mathrm{mix}/cPD}$ differ less than ±4 m (Figure 8a); $h_{\mathrm{mix}/cS}$ and $h_{\mathrm{mix}/cPD}$ by less than ±5 m and $h_{\mathrm{mix}/cS}$ and $h_{\mathrm{mix}/cT}$ by less than ±8 m (Figures 8b and 8c). The distribution of the difference between $h_{\mathrm{mix}/cT}$ and $h_{\mathrm{mix}/cPD}$ has a median very near zero (Figure 8b). In contrast, the difference between $h_{\mathrm{mix}/cS}$ and $h_{\mathrm{mix}/cPD}$ is skewed toward larger $h_{\mathrm{mix}/cPD}$ (Figure 8a); the difference between $h_{\mathrm{mix}/cS}$ and $h_{\mathrm{mix}/cT}$ shows a small skew toward larger $h_{\mathrm{mix}/cT}$, with a median at −1 m (Figure 8c). In general, changes in temperature and salinity in the surface layer seem to be density compensating that we find larger isothermal layers than isohaline layers, with isopycnal layers in between. For the compensation of horizontal temperature and salinity gradients in the ocean mixed layer on scales from 10 m to 100 km we refer to, e.g., *Rudnick and Ferrari* [1999].

[42] The global map where the differences between the CTD profiles from Figure 8 equal 70% shows that the regions with high values (>15 m) occur in the western and central tropical and North Pacific (Figures 9b and 9c). Large differences between $h_{\mathrm{mix}/cS}$ and $h_{\mathrm{mix}/cPD}$ extend farther northward along the western boundary of the North Pacific (Figure 9c). Larger horizontal gradients of h_{mix} derived from the different techniques appear within eddies of the Kuroshio compared those within the Gulf Stream [*Kara et al.*, 2000a]. Both the deep saline layer as well as the barrier

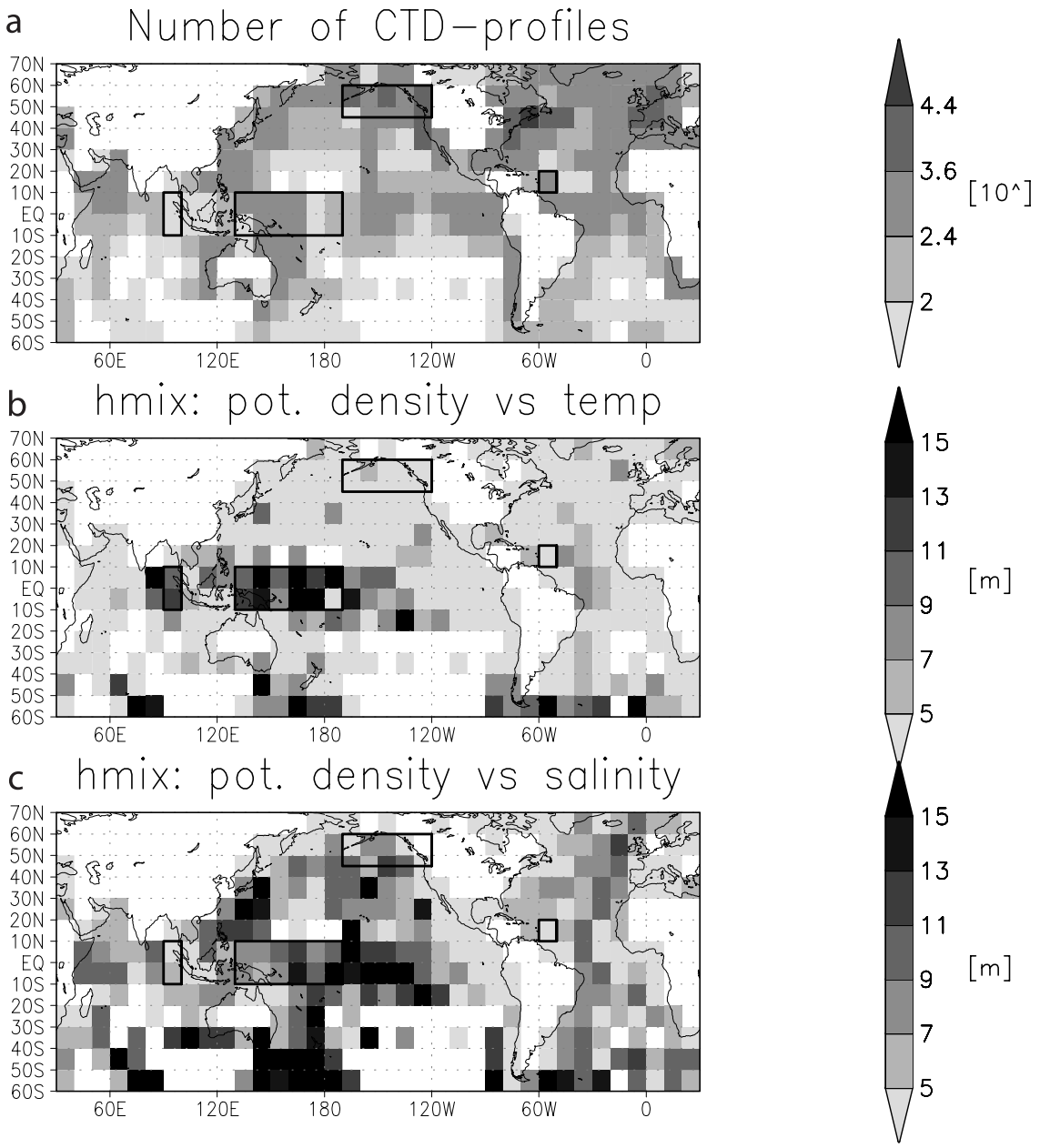

Figure 9. (a) Number of CTD profiles binned in 10° × 10° boxes. First value where the integrated error between $h_{mix/c}$ inferred from (b) potential density and temperature profiles and (c) potential density and salinity profiles, respectively, exceeds the 70% interval (white, undefined values). Boxes marked by a black line indicate barrier layer regions [*Sprintall and Tomczak*, 1992; *Kara et al.*, 2000a].

layer act to define $h_{mix/cS}$ in the western tropical Pacific. During the onset of the 1997–1998 El Niño, zonal advection of fresh water from the west was particularly important in the central equatorial Pacific [*Wang and McPhaden*, 2001], so shallow wind-driven currents form vertical layers of density that not necessarily reflect the local effects due to forcing by rain and heating. In general, regions in the tropics and northwestern Pacific, where large differences between isohaline and isopycnal methods are found, coincide with fresh water barrier layer regions [*Sprintall and Tomczak*, 1992; *Kara et al.*, 2000a]. There the generation of turbulence is due to both changes in local surface fluxes as well as strong upper ocean currents (Figure 9a).

3.2. Effects of Low Vertical Resolution

[43] Low vertical resolution of observed or simulated data has a significant impact on estimating h_{mix} (see section 2.2.1). In order to evaluate the effect of low vertical resolution we artificially reduced CTD profiles to a 20-m vertical resolution and estimated h_{mix} based on both low- and high-resolution profiles. The results of this comparison are presented below. Additionally, we estimated h_{mix} based on the output of an OGCM, with low nonlinear vertical resolution (section 5).

[44] In order to estimate the error of $h_{mix/c}$ computed from low-resolution profiles we assume that $h_{mix/c}$ computed from high-resolution temperature and potential density

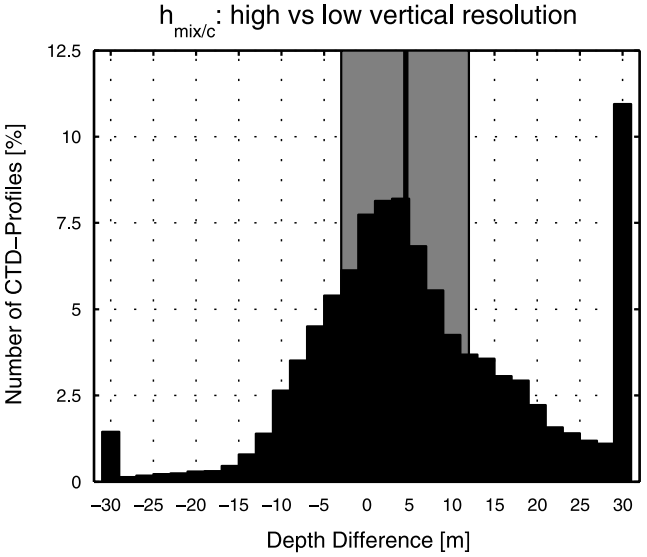

Figure 10. Histogram of the difference between $h_{mix/c}$ of low- (20 m) and high- (2 m) resolution CTD-temperature profiles (bins, 2 m; negative, deeper $h_{mix/c}$ from high-resolution profiles). The shaded area marks the 50% interval around the median (black line) of the distribution (median, 5 m; m50, 8 m). Analyses for σ_Θ show a similar behavior.

profiles represent the real depth of the ocean mixed layer. The median of the differences between $h_{mix/c}$ computed from low-resolution profiles and that computed from high-resolution profiles is 5 m; half of the differences lie within ±8 m around the median (Figure 10). This is a significantly smaller value if compared to the accuracy in $h_{mix/d}$ of ±20 m in 85% of the cases found by *Kara et al.* [2000b] (applying the 0.8°C criterion to monthly climatological profiles). However, the distribution of the differences show a skew toward an overestimation of using low-resolution data as 12% of the low-resolution computations are larger by more than 30 m, but only 1% are smaller by more than 30 m (Figure 10).

[45] A most remarkable feature in both the Δ as well as the curvature methods of computing h_{mix} in the 20-m vertical resolution and the 2-m CTD-temperature profiles are the clustering, or stickiness of h_{mix} to the sampling levels (Figure 6). The behavior of the distribution function of $h_{mix/c}$ shows a more sinusoidal behavior than $h_{mix/d}$ even if these have similar amplitudes. Therefore the $h_{mix/d}$ has concentration peaks at the sampling levels indicating a stronger clustering around the levels, in contrast to the structure of $h_{mix/c}$ (see Figure 3d).

[46] In general all the algorithms endeavor to reconstruct a nonlinear parameter h_{mix} from the discrete profile data. From among those algorithms we investigated, perhaps the best choice is one that produces the smallest bias relative to some simple, "continuously" sampled profiles. A linear interpolation between the levels leads to shallow biases, an underestimation of h_{mix} and it seems to cluster calculations around the shallower level of the interpolation interval, respectively (see Figure 3c). This bias decreases with increasing vertical resolution, but does not altogether avoid stickiness around the layers where data sampled. There is some improvement with an exponential interpolator. The curvature-based algorithm dramatically improves the stickiness in the midlatitudes, especially in summer and fall. Stickiness occurs primarily in the tropics where the daily average profiles appear to have smooth transitions from the weakly stratified, strongly turbulent layer to the top of the less turbulent main thermocline (see Section 2.3).

[47] Note, in general it is difficult to address $h_{mix/c}$ or $h_{mix/d}$ based on low-resolution profiles as the more reliable estimate for the real h_{mix}. Assuming $h_{mix/c}$ from high-resolution profiles to be representative for the real h_{mix} the histogram of differences between the real h_{mix} and $h_{mix/d}$ based on low-resolution profiles shows the same scattering like the corresponding $h_{mix/c}$ (see Figure 6). However, the explained variance (squared correlation coefficient) between $h_{mix/c}$ based on high- and low-resolution profiles amounts to 72% and to 46% for $h_{mix/c}$ based on high- and $h_{mix/d}$ based on low-resolution; this seems to indicate that $h_{mix/c}$ based on low-vertical resolution profiles is more reliable than the corresponding $h_{mix/d}$. In addition to determining the correct measured level from where to interpolate to estimate $h_{mix/c}$, the exponential interpolator appears to be responsible for an $h_{mix/c}$ based on low-resolution profiles (even if it clusters around sampling levels) that shows a higher correlation with the real h_{mix} and that $h_{mix/c}$ is not "just somewhere" between two or at one sampling level like the corresponding $h_{mix/d}$.

3.3. Biases of Climatologies From MBTs and T/T Array

[48] In order to analyze the sensitivity of $h_{mix/c}$ with respect to temporal averaging we calculated $h_{mix/c}$ from daily MBT-temperature profiles in the western North Pacific in the 1° × 1° area centered at 31°N, 164° (OWS-V) during July 1954. The monthly mean $h_{mix/c}$, based on daily average data, is 15.8 m (black solid line in Figure 11); in contrast, the mean $h_{mix/c}$ computed from the monthly mean profile is

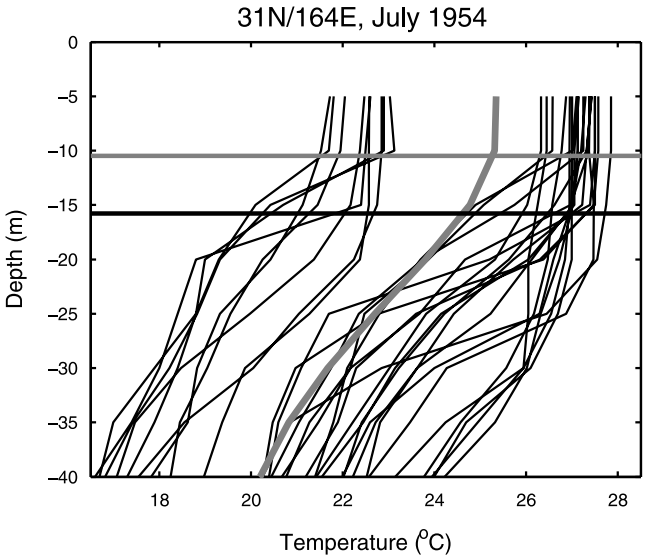

Figure 11. Daily MBT-temperature profiles and corresponding monthly mean $h_{mix/c}$ (black lines) at 164°E/31°N (July 1954); the successive profiles are shown with an offset of 0.025°C for a clearer picture. Monthly mean temperature profile and corresponding $h_{mix/c}$ (gray lines).

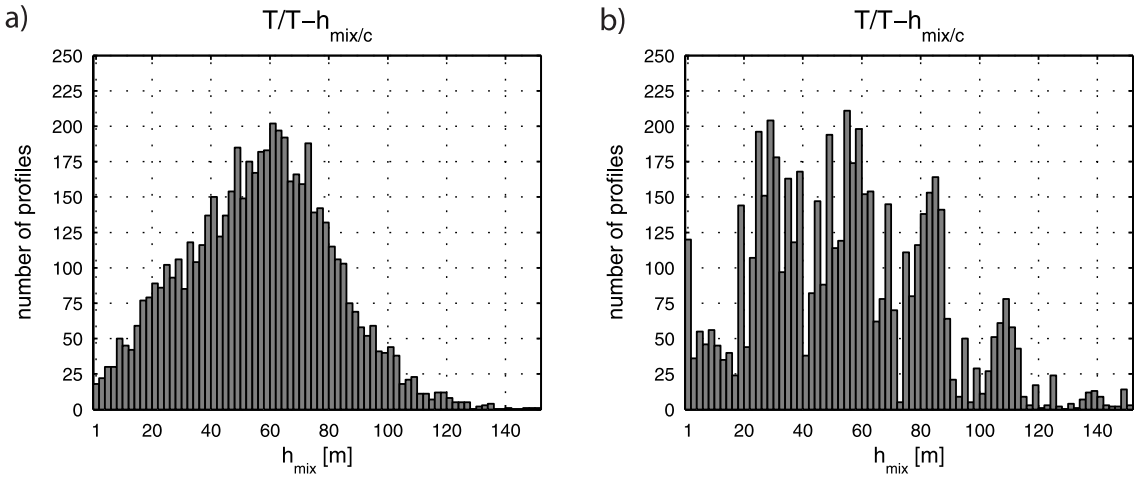

Figure 12. Histogram of monthly mean $h_{mix/c}$ inferred from temperature profiles of the T/T array (with depth bins, 2 m): (a) daily and (b) monthly mean profiles, respectively (the vertical resolution (~20 m) left unchanged). (Vertical grid lines mark mean depths of the sensors.)

10.4 m (gray solid line in Figure 11). The resulting difference of 5.4 m is significant because the standard deviation of the daily $h_{mix/c}$ was 5.1 m. The result from *de Boyer Montégut et al.* [2004] confirm the shallow bias of $h_{mix/c}$ based on averaged profiles compared to $h_{mix/c}$ derived from in situ data. The authors constructed a global climatology of $h_{mix/d}$ (with $\Delta T = 0.2°C$) based on averaged temperature profiles which is 25% shallower than $h_{mix/d}$ estimated from individual profiles.

[49] From daily average, 20-m resolution temperature profiles of the T/T array we calculate $h_{mix/c}$ and average these to monthly means. The main effect of temporal averaging of a profile appears to be the smoothing of the vertical gradients at the base of h_{mix} and a "broadening" of

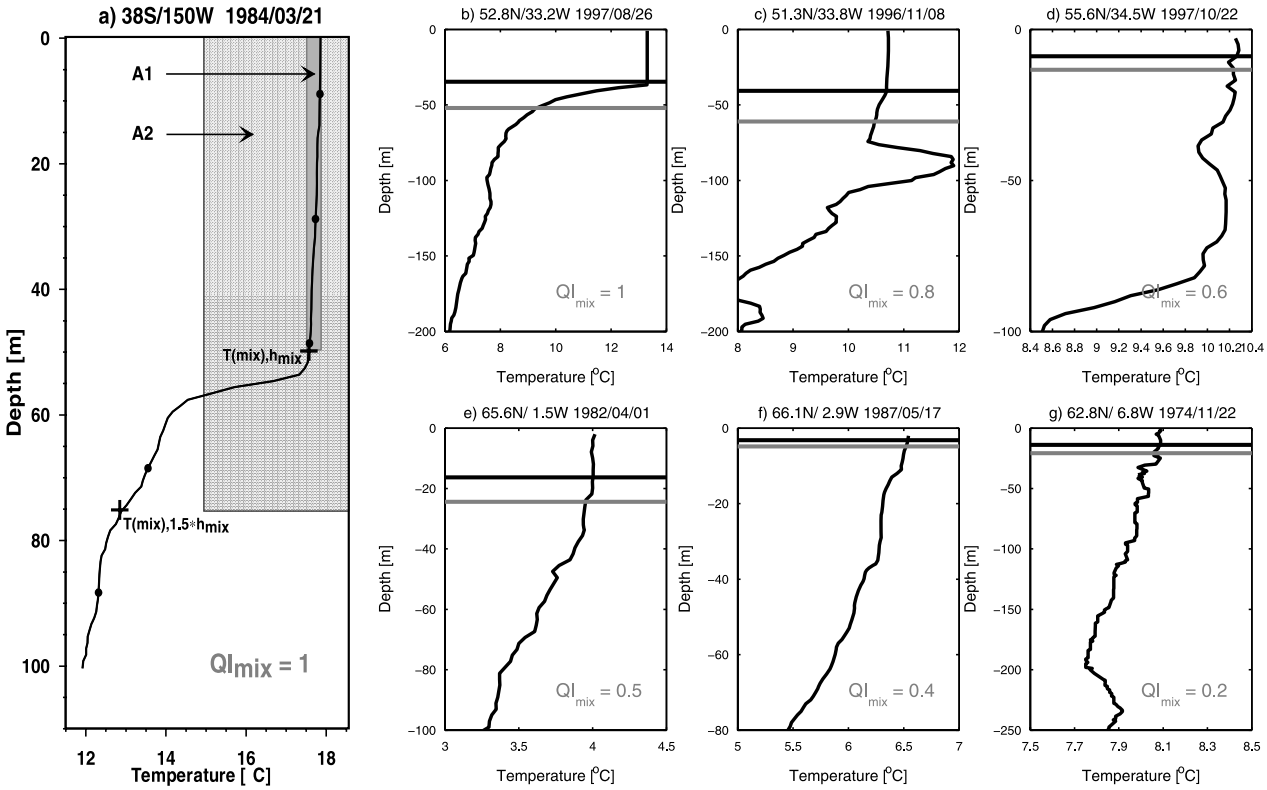

Figure 13. (a) Sketch of our quality index QI_{mix} of h_{mix}. (b)–(g) Corresponding CTD-temperature profiles for different QI_{mix}. Black solid lines mark $h_{mix/c}$ and gray solid lines mark 1.5 × $h_{mix/c}$, respectively.

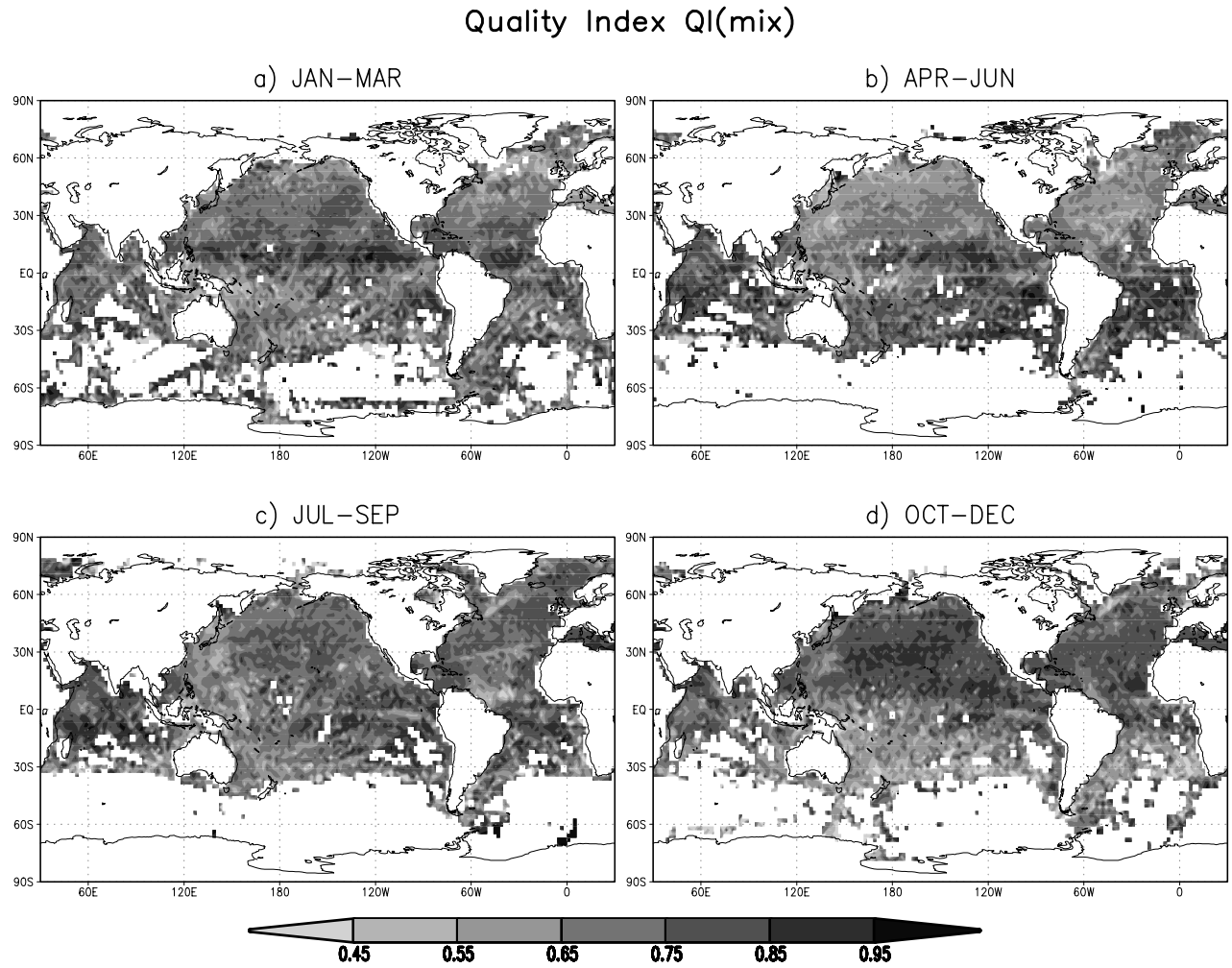

Figure 14. Quality index QI_{mix} of $h_{mix/c}$ (see Figure 15a) (white, undefined values).

the seasonal thermocline. As above, we calculate monthly mean profiles and from these $h_{mix/c}$ (see section 2.1). As at OWS-V, monthly averaging of the T/T profiles results in a shallow $h_{mix/c}$ bias. This averaging also appears to enhance the accumulation of $h_{mix/c}$ around the sampling intervals (Figure 12). However, this accumulation is significantly reduced in the monthly average, even in low-resolution profiles, if daily data on $h_{mix/c}$ are available for computing its monthly mean (Figure 12).

3.4. Quality Index, QI_{mix}

[50] Calculating h_{mix} is based on the notion that there exists a near-surface layer with quasi-homogeneous properties in which the standard deviation of the property about its vertical mean is close to zero. Below the depth of h_{mix}, property variance should increase rapidly about its vertical mean. A quality index for h_{mix} by which we can quantify if this assumption is valid is the ratio of the standard deviation of the observed property in the depth range from the surface to h_{mix} to the standard deviation from the surface to the depth of $1.5 \times h_{mix}$ (namely, Figure 13a). The analysis of the observed profiles showed that the depth $1.5 \times h_{mix}$ is a realistic choice for including most of the upper ocean stratification and not intruding into the main thermocline. We subtract the standard deviation ratio from 1.0 so that a value of 1.0 represents high-"quality" computation of h_{mix} and progressively lower values imply that larger volumes of stratified water are present above the level of h_{mix} (equation (4) and Figure 13a). Consider the quantity, QI_{mix}, as

$$QI_{mix} = 1 - \frac{A1}{A2} = 1 - \frac{\sigma(T_n - \langle T \rangle)|_{(h_1, h_{mix})}}{\sigma(T_n - \langle T \rangle)|_{(h_1, 1.5 \times h_{mix})}}, \qquad (4)$$

where $\sigma(\ )$ denotes the standard deviation from the vertical mean $\langle\rangle$ from h_1, the first layer near the surface, to the depth of h_{mix} or $1.5 \times h_{mix}$, respectively.

[51] The examples of values from different CTD temperature profiles (Figures 13b–13f) demonstrate that if $QI_{mix} > 0.8$ a well defined h_{mix} results. For QI_{mix} in the range 0.5–0.8, increased uncertainty of the profile interpretation becomes evident and with $QI_{mix} < 0.5$ no mixed layer interpretation is possible. We also find that QI_{mix} for $h_{mix/d}$ is in average 10% smaller than for $h_{mix/c}$ indicating that the curvature methodology is more robust. The spatial pattern of QI_{mix} for $h_{mix/c}$ for different seasons shows that in most regions of the world ocean QI_{mix} is above 0.7, for about 70% of the profiles (Figure 14). Predictably, QI_{mix} has the largest values in the hemispheric summer and fall

when a sharp gradient at the base of the seasonal mixed layer is present. The reason why a lower value of QI_{mix} occurs where a barrier layer and near the eastern Pacific equator is that in the former a quasi-homogeneous column exists below the barrier layer and strong equatorial upwelling and daily vertical mixing cycles produce significant layering near the equator. On the basis of the stringent criteria introduced here, it makes little sense to refer the equatorial mixed layer as determined from T/T array, or any limited vertically sampled temperature profiles as the region of enhanced turbulence. In subpolar regions, mainly in the North Atlantic during winter, QI_{mix} is also seen to fall below 0.5 (Figure 14a); this reflects that convective mixing is not going on and ''wriggly'' profiles or small vertical gradients exist throughout the water column that make the turbulent layer determination on the basis of profile data somewhat problematic (Figures 2h, 2i, and 13d–13f).

4. Characteristics of Observed Mixed Layer Depth Variability

4.1. Global Features

[52] The pattern of seasonal mean $h_{mix/c}$ computed from the global individual profile data (Figure 1) shows the familiar negative zonal gradients in equatorial regions throughout the year with shallow $h_{mix/c}$ (<40 m) in the east and deeper $h_{mix/c}$ (>100 m) in the west; the shallow $h_{mix/c}$ in the eastern equatorial Pacific is reproduced in a broader tongue during the first half of the year (Figure 15a, January–March and April–June). In the winter and springtime North Pacific a band of $h_{mix/c} < 75$ m is found around 30°N from the west coast to 150°W that is shallower than the surrounding $h_{mix/c}$ (Figure 15a, January–March and April–June). This is due to the occurrence of the subtropical front under which the mixed layer remains shallow even in strong winds that produce deep mixed layers to its north and south [*Niiler*, 1982]. This band disappears in summer where $h_{mix/c} < 40$ m north of about 25°N (Figure 15a, July–September). A local maximum of $h_{mix/c}$ (>100 m) appears in winter west of Peru near 25°S, 110°W (Figure 15a, July–September). *Tomczak and Godfrey* [1994] (with ΔT = 0.5°C) find a similar distribution. A radial pattern is found in $h_{mix/c} > 100$ m that reflects the subtropical gyre structure (Figure 15a, July–September).

[53] The data distribution at the time of writing this report significantly limits the computation of significant seasonal means of h_{mix}, especially in high latitudes with weak stratification conditions as for example in the Labrador Sea in winter. There the winter data is composed mainly of XBT profiles that sample to 1000 m. These depict obvious mixed layers near the surface, but without salinity compensating effects, the turbulent layer cannot be determined. Convection to the level of Labrador Seawater formation to 1500 m and below cannot be sampled by these relatively shallow temperature profiles. Therefore our results of a long-term seasonal mean $h_{mix/c}$ and its standard deviation are biased by under sampling and the lack of salinity observations in many regions. In the Labrador Sea the bias is toward shallower $h_{mix/c}$ and smaller standard deviations than we believe should occur from a knowledge of the physical processes observed in concentrated field experiments [e.g., *Krahmann et al.*, 2003]. *De Boyer Montégut et al.* [2004] identify a maximum winter $h_{mix/d}$ (ΔT = 0.2°C) based on individual profiles in deep water formation regions that is significantly shallower that previous estimates. This indicates that variations of h_{mix} are detected instead of deep thermocline movements. However, It goes without saying that an expert oceanographer must consider the data in each ocean region and global pictures, as presented here, must be used only as points of departure for more thorough investigations.

[54] The historical data (see Figures 1 and 9a) is relatively comprehensive in many regions and we provide the seasonal means and the standard deviation of anomalous monthly mean as a base from which to embark for future research. The standard deviations of anomalous monthly mean $h_{mix/c}$ in the 2° × 2° boxes are defined only if more than 4 values in a calendar month exist. Recall that the variance (standard deviation squared), in addition of direct forcing from the atmosphere, can be produced both by internal waves and ocean eddies that move the mixed layer vertically and horizontally on short timescales.

[55] The variance of $h_{mix/c}$ is largest (>50 m) in the mode and deep-water formation regions in both hemispheres in winter and also in the Northern Hemisphere spring (Figure 15b, January–March and July–September). However, generally, the variance is largest in the Southern Ocean due to temporal data gaps. Once the seasonal thermocline is formed in midlatitudes, the variability of $h_{mix/c}$ is less then 10 m in summer, increases slightly to the largest value of 20 m in fall (Figure 15b). In the band around 30°N in the Pacific, where $h_{mix/c} < 80$ m in winter, the variability exceeds 25 m (Figure 15b, January–March). Farther south (around 10°N) $h_{mix/c}$ is about 100 m and its variability <20 m. This is the region of the North Equatorial Counter Current that flows against the prevailing Trade winds and the turbulence is active there throughout the year. The variability of $h_{mix/c}$ in the equatorial Pacific is about 25 m in the west and is less than 10 m in the east over the entire year (Figure 15b) but recall the caveat of interpreting the quasi-homogeneous layer on the equator as a region of active turbulence.

[56] In general, the pattern of the anomalous monthly mean $h_{mix/c}$ reflects the one from the long-term seasonal mean: the larger the mixed layer depth the larger its monthly mean anomaly. Consider also the standard deviation of $h_{mix/c}$ relative to its seasonal mean value that takes into account also effects of a variety of short-term vertical and horizontal adiabatic heaving of the seasonal and main thermoclines. The largest relative variance (>30%) appears in the northern hemispheric spring when the seasonal $h_{mix/c}$ is small (Figures 15a, January–March, and 15c April–June); the smallest relative variance (<20%) is in the Northern Hemisphere autumn (Figure 15c, October–December). These patterns reflect either a higher sensitivity of the technique for computing $h_{mix/c}$ during the seasonal thermocline formation that occurs during the demise of the seasonal thermocline, or quite simply upper ocean inhomogeneities are large when the mixed layer is small.

4.2. Equatorial Pacific Ocean From T/T Array

[57] To view a more detailed description of the seasonal-to-interannual variability of $h_{mix/c}$, consider the longitude-

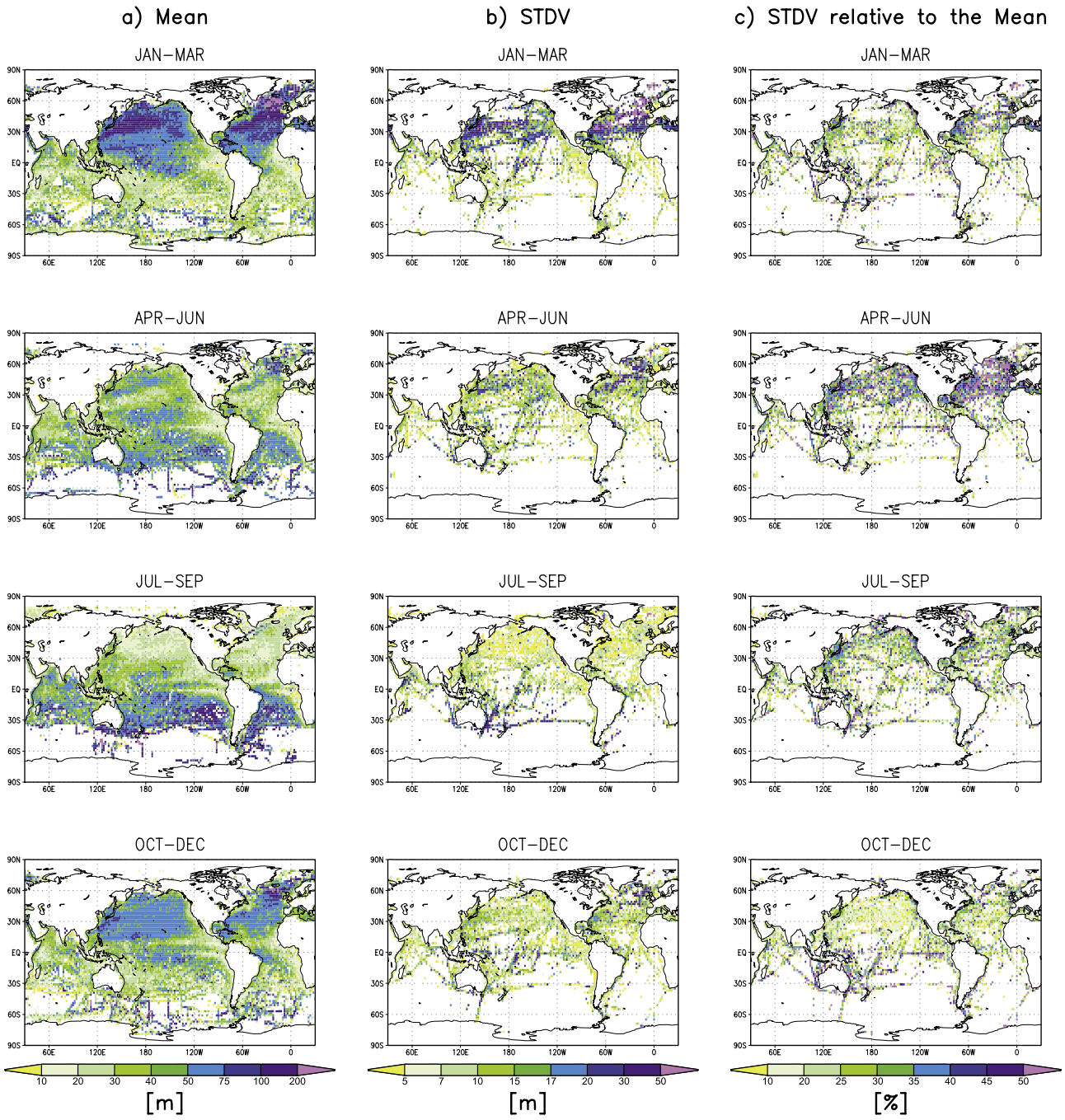

Figure 15. Ocean mixed layer depth $h_{mix/c}$ for different seasons: (a) long-term mean, standard deviation of anomalous monthly means: (b) absolute and (c) relative to the long-term monthly mean for combined CTD-XBT data (white, undefined values).

time diagram of anomalous monthly mean $h_{mix/c}$ computed from the T/T array (Figure 16a); whereas anomalies of monthly mean $h_{mix/c}$ define deviations from the long-term monthly mean climatology of $h_{mix/c}$. The phase and amplitudes of anomalous $h_{mix/c}$ in the equatorial Pacific are dominated by the 1997–2000 El Niño/La Niña cycle. During the build up of El Niño a positive anomaly of $h_{mix/c}$ propagates eastward where it reaches its maximum after 12 months. During the La Niña period a maximum negative anomaly also spreads eastward as its amplitude decreases. During the termination of La Niña in 2000 a systematic increase of $h_{mix/c}$ occurs in the west and a decrease in the east, with an inflection point 150°W. The El Niño/La Niña cycle of 1992 to 1996 appears to be stationary with no propagations features that can be readily identified. During the build up of El Niño there is a decrease

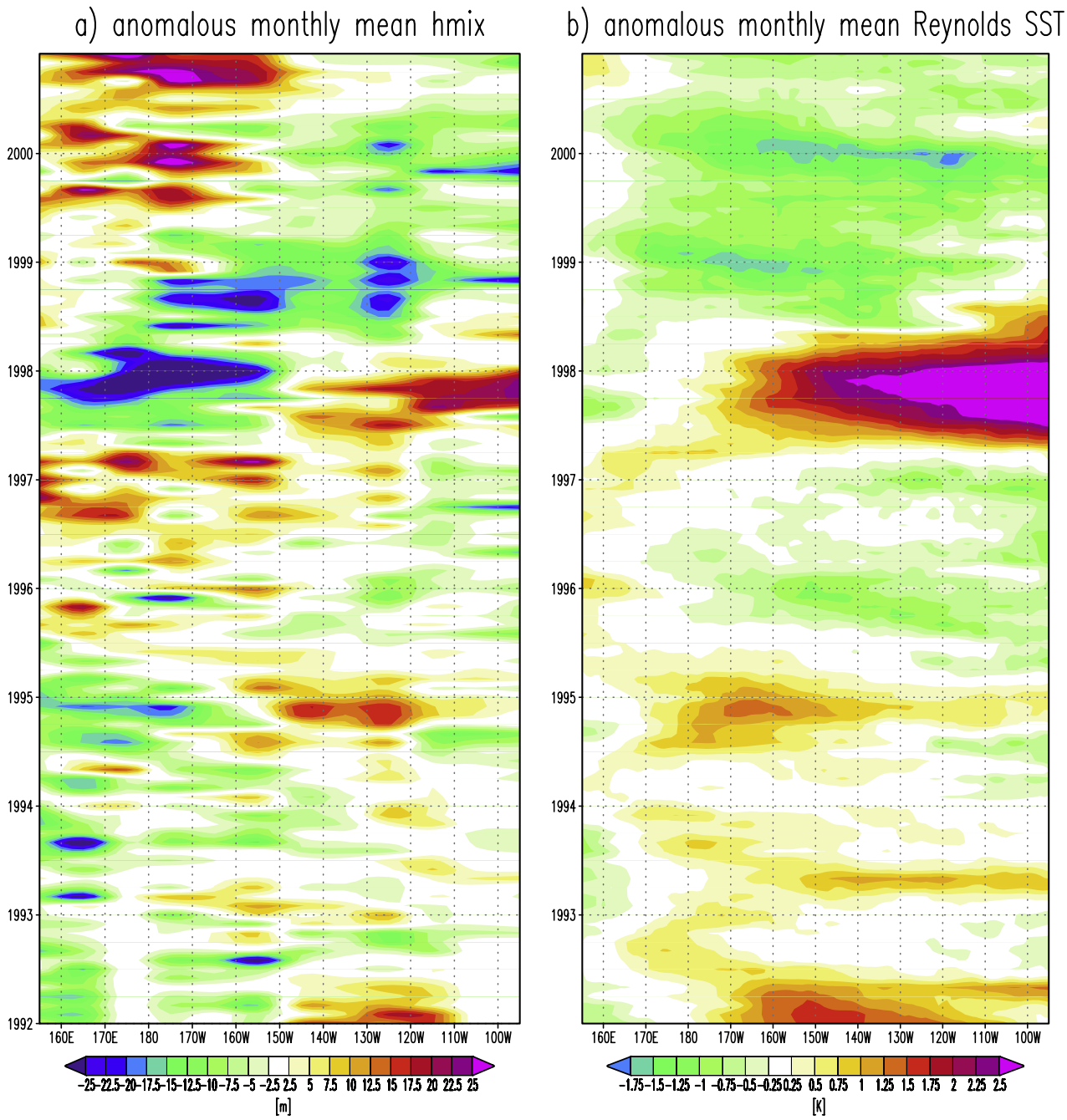

Figure 16. (a) Hovmøller diagram of anomalous monthly mean $h_{mix/c}$ (defined by the present study) in the tropical Pacific (meridionally integrated between 8°S–8°N and based on daily temperature profiles of the T/T array) (positive, deepening of h_{mix}). (b) Corresponding evolution of anomalous monthly mean SST after Reynolds [*Reynolds and Smith*, 1994].

of $h_{mix/c}$ in the west and slight increase in the east; the La Niña period is marked by the opposite behavior with the inflection point again at 150°W. The corresponding SST anomalies (namely, http://www.cdc.noaa.gov/cdc/data.reynolds_sst.html) depict a strong warming of the "cold tongue" in 1997 that coincides with the largest increase of $h_{mix/c}$. Unlike the $h_{mix/c}$, the 1997–2000 SST anomalies show no propagation during both El Niño and La Niña phases. The propagating anomalies of $h_{mix/c}$ toward the east might be more related to the propagating character of the top of the main thermocline, for as has been explained above, the computation of $h_{mix/c}$ in the equatorial zone identifies the location where the weak upper ocean temperature gradient changes to a larger value at the top of the main thermocline.

[58] In the tropical Pacific area that is spanned by the T/T array, the zero lagged correlation between anomalous monthly mean $h_{mix/c}$ and the SST as average over the eastern region is locally positive around 0.6; the largest lagged negative correlation (<0.3) is in a region northwest

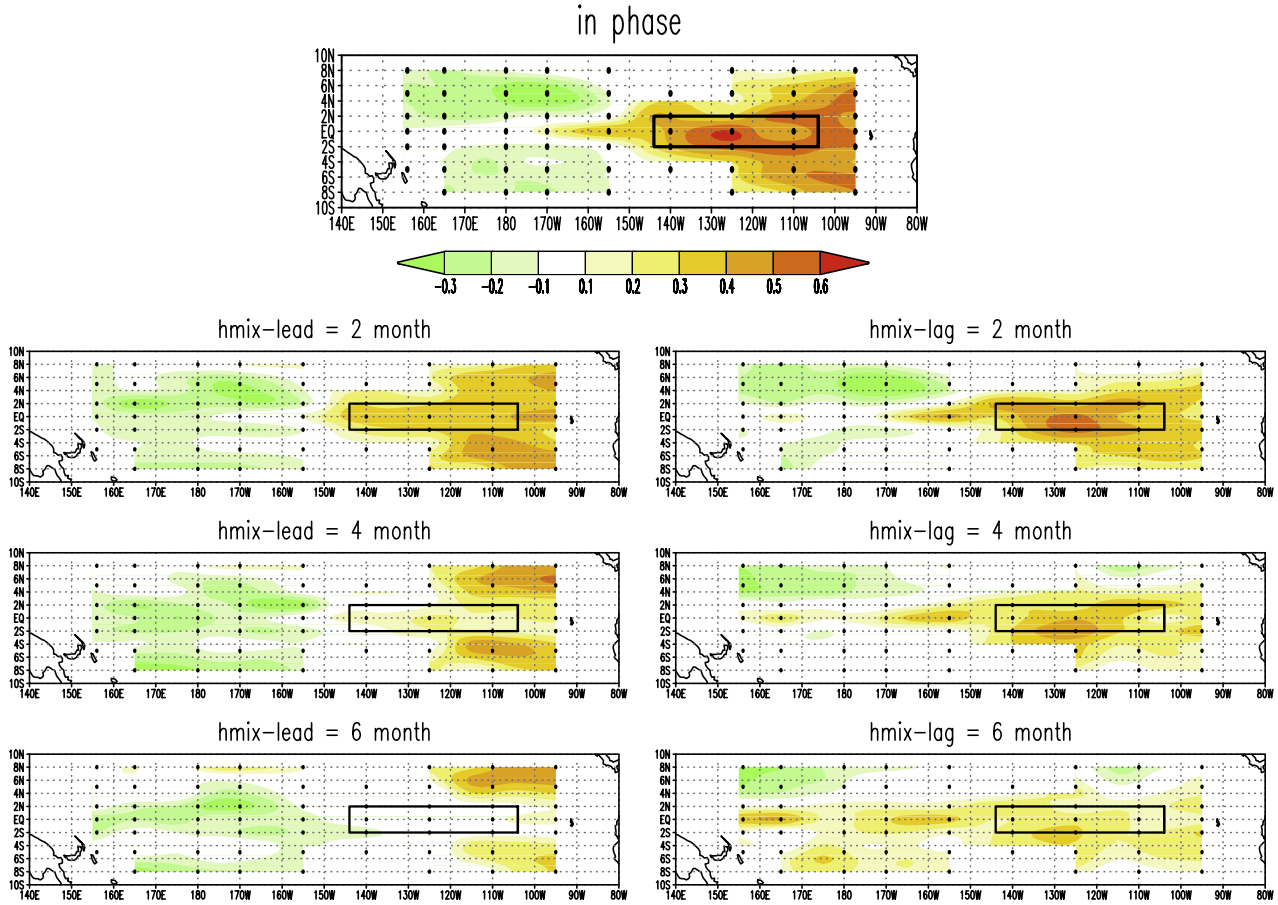

Figure 17. Anomaly correlation of monthly mean $h_{mix/c}$ and SST in the box in the tropical Pacific for different time lags (based on daily temperature profiles of the T/T array). The box defines the area between 2°S and 2°N/104–144°W; dots indicate the position of the T/T buoys.

of the SST box (Figure 17). This negative maximum, though barely significant at the 95% level, moves toward the equator and becomes less extensive zonally as $h_{mix/c}$ leads. The local positive correlation disappears if $h_{mix/c}$ leads by 6 months (Figure 17, left). In terms of equation (1), it is thus apparent that the SST anomaly evolution is not well predicted by a one-dimensional heat storage processes because there should be a maximum of the correlation with $h_{mix/c}$ leading by 3–9 months.

5. Characteristics of ECCO Simulated Mixed Layer Depth Relative to $h_{mix/c}$

[59] It is one aim of this manuscript to develop a criterion for h_{mix} that can be comparably applied to not only observational but also to model data. Therefore the following analysis of an OGCM model output does not only compare the model simulations with observations, but also highlights the skill of the estimated h_{mix}. The model study has, in respect to the skill of the h_{mix} estimation, the additional advantage that the true mixed layer depth can be diagnosed directly, which makes the evaluation of the skill of our method estimating h_{mix} more objective. From the 1° × 1° global ECCO state estimation (see section 2.1) we use daily average potential temperature profiles to compute both $h_{mix/c}$ and $h_{mix/d}$, after which the monthly means are calculated. ECCO uses the *K* profile parameterization (*K*PP) for near-surface vertical diffusion coefficients [*Large et al.*, 1994]. The *K*PP scheme diagnoses an "oceanic planetary boundary layer depth" (h_{pbl}) that is defined as that depth where the "bulk Richardson number" exceeds a critical value (>0.3) [*Menemenlis et al.*, 2005]. This is the "depth of mixing due to turbulent velocities of unresolved eddies" [*Large et al.*, 1994, p. 1524]. Below this depth, in the ocean interior, the *K*-mixing profiles of the *K*PP model depend on a number of processes which are: shear instability, background internal wave activity, and static instability. These processes enhance the mixing coefficients and therefore may lead to larger h_{mix} than predicted by h_{pbl} alone. Thus ECCO model computes the time evolution of vertical profiles of upper ocean temperatures both from assimilation of the instrumental observations, like T/T array data, and from the direct application of the *K*PP upper ocean mixing scheme.

[60] In general, the ECCO simulated $h_{mix/c}$ and $h_{mix/d}$ are in fact always larger than h_{pbl}. Largest differences are found throughout the year in the band of the T/T array, ±10° around the equator and west of the boundary upwelling regions. On the global scale, $h_{mix/c}$ is usually less than 40% larger than h_{pbl}, but the relative differences between $h_{mix/d}$ and h_{pbl} are often greater than 50% (not shown). Because there are not very many instrumental observations of

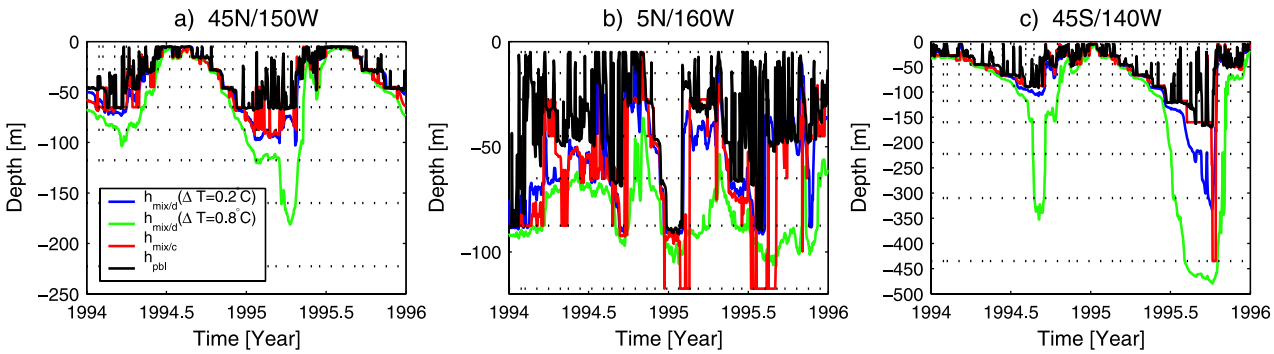

Figure 18. Time series of simulated mixed layer depth $h_{\mathrm{mix}/d}$ ($\Delta T = 0.2°\mathrm{C}$ and $\Delta T = 0.8°\mathrm{C}$) and $h_{\mathrm{mix}/c}$ (blue, green, and red lines, respectively) as well as (black line) the modeled oceanic planetary boundary depth h_{pbl} at three different grid points: (a) midlatitudinal central Pacific, (b) equatorial central Pacific, and (c) Southern Ocean; dotted lines indicate the model levels.

temperature in the midlatitudes, as expected, the time series of simulated $h_{\mathrm{mix}/c}$, $h_{\mathrm{mix}/d}$ and h_{pbl} at many different locations in the midlatitudes display a remarkable correlation between their phases and amplitudes (Figures 18a and 18c); the fluctuations of $h_{\mathrm{mix}/c}$ follow closely the high-frequency, daily changes in h_{pbl}. In the hemispheric winters, where the mixed water column achieves largest values, $h_{\mathrm{mix}/c}$ appears to capture simulated mixing events of *K*PP very well. At the same time, a large Δ criterion fails to find the depth of *K*PP mixing (Figures 18a and 18c), whereas smaller Δ criterion seems to get the right h_{pbl} but shows less high-frequency variability than h_{pbl}. Over the global domain, which excludes the equators, and independent of the season and chosen ΔT, $h_{\mathrm{mix}/d}$ is generally larger than $h_{\mathrm{mix}/c}$ or h_{pbl} and the distribution function of $h_{\mathrm{mix}/d}$ decays in a smoother fashion, particularly for a larger Δ criterion. The distribution functions of all the three turbulent layer depths are similar in shape to the observed distribution function (namely, Figures 6 and 19). The correlation between anomalous monthly mean simulated h_{mix} and h_{pbl} is always positive and for $h_{\mathrm{mix}/c}$ it is >0.8 on a global scale (not shown). The corresponding correlation for $h_{\mathrm{mix}/d}$ is somewhat weaker, in particular poleward of 40° and in the equatorial region it is less than 0.4.

[61] Around the equator the daily variations of the modelled vertical mixing depth are not well reproduced by either method of estimating how deep *K*PP mixes (Figure 18b). This is an indication that in the Pacific, ECCO often prefers to choose the assimilated T/T data for its profiles, on top of which *K*PP produces a turbulent "quasi-homogeneous" upper layer that does not appear to be very often the layer assimilated from T/T array into ECCO.

[62] In comparison with the observed $h_{\mathrm{mix}/c}$, the ECCO simulated $h_{\mathrm{mix}/c}$ appear to be generally smaller by around 30% for all seasons (Figure 20). Along the equator the simulated $h_{\mathrm{mix}/c}$ is even smaller where relative difference between observed and simulated $h_{\mathrm{mix}/c}$ exceeds 50% throughout the year (Figure 20). Exceptions to these general patterns are at the mode and deep-water formation regions, in the Kuroshio, Gulf Stream extensions and the convective regions of the Northern Hemisphere in winter (Figure 20a) and in the Southern Ocean during winter and spring (Figures 20c and 20d), where larger simulated $h_{\mathrm{mix}/c}$ occur than are observed. We find that while in general the relative differences between the observed and simulated $h_{\mathrm{mix}/c}$ were less than 10% this could well be due to the assimilation by ECCO of the data we used to compute the observed values. The h_{pbl} generated by ECCO is very much smaller than the observed value of $h_{\mathrm{mix}/c}$. ECCO mixes the ocean vertically by assimilation, or by a background vertical diffusivity, more than it does by *K*PP.

6. Summary and Discussion

[63] In this study we established a new criterion to identify the depth to which homogenization occurs in the upper layer of the ocean, $h_{\mathrm{mix}/c}$. The criteria uses, together with some boundary conditions, the first maximum of curvature of the temperature and density profiles to identify h_{mix}. Two advantages of this approach are as follows: (1) The empirical specified parameters are independent from another dynamical quantity, such as the SST. (2) The estimated h_{mix} is not a linear function of any of the

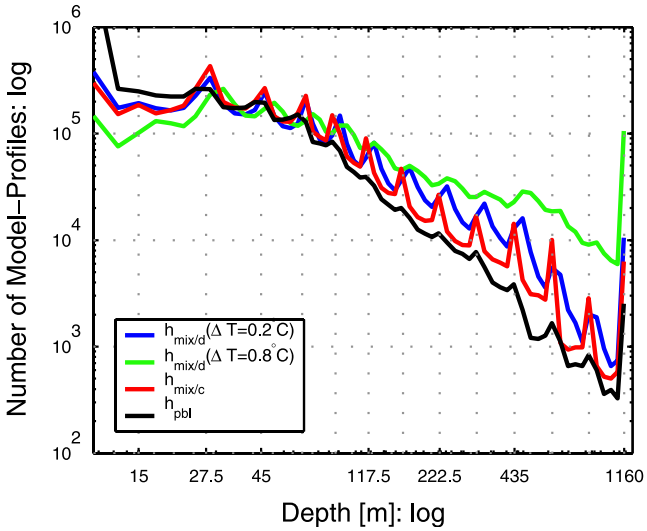

Figure 19. Distribution of the depths described in Figure 18 for the complete model domain (depth bins, 5 m); vertical dotted lines represent the model levels.

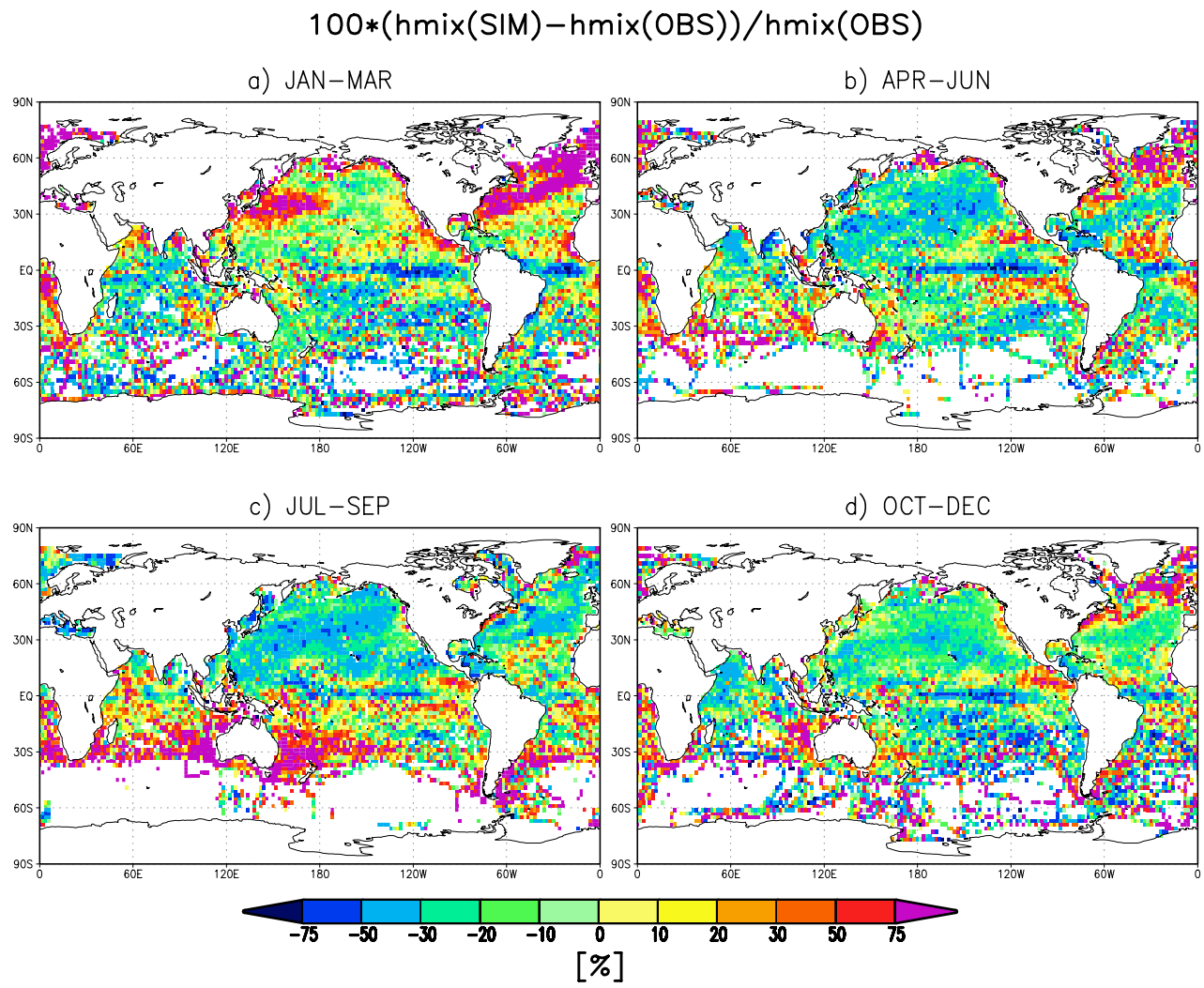

Figure 20. Percentage normalized difference between simulated and observed monthly mean $h_{mix/c}$ (negative, deeper observed $h_{mix/c}$; white, undefined values).

empirical parameters, as it is the case for $h_{mix/d}$ based on a Δ criterion. The method has been developed empirically on the basis of a global data set of around 5 million MBT, XBT, and CTD profiles as well as the output of the MIT-OGCM, the $1^\circ \times 1^\circ$ global ECCO state estimation. This curvature criterion appears to be more universally applicable in both data and model computations of the mixed layer depth, h_{mix}, compared to an algorithms that utilize a Δ criterion. We made an effort to prove the curvature criterion as systematic as possible, which includes, amongst others, the application of the criterion to both idealized and individual observed profiles with different vertical resolution, the definition of a quality index, QI_{mix}, for h_{mix} and comparisons to h_{mix} based on simulated profiles.

[64] For simplified, but realistically shaped profiles, the curvature criterion, when combined with the exponential interpolation routine, eliminates the weaknesses of the Δ criterion. In about 70% of the observed high-resolution CTD profiles, the $h_{mix/d}$ that are based on the Δ criterion show the systematically overestimation compared to $h_{mix/c}$ based on the curvature criterion.

[65] For about two thirds of all individual profiles we found $h_{mix/c}$ to be more reliable in separating regions of low- (well mixed) and high- (stratified) temperature variance. Using a $\Delta T = 0.2^\circ$C (following *de Boyer Montégut et al.* [2004]) $h_{mix/d}$ appears to be superior of $h_{mix/c}$ in 10% of the profiles. For the remaining percentage it is not definite which one of the two criteria selects the optimal quasi-homogeneous layer. In general, a Δ criterion seems to encroach into the stratified layer below depending upon the value Δ chosen; a single value of Δ produces $h_{mix/d}$ with dependencies on the ocean region and season of the year. For example, if an appropriate value of Δ for the midlatitude summer is used, in higher latitude hemispheric winter and spring, $h_{mix/d}$ values are often too large as this algorithm wrongly identifies a significant part of the top of the weak main thermocline as belonging to the mixed layer. Even a, relatively small, global uniform $\Delta T = 0.2^\circ$C does often not capture small vertical gradients indicating the base of deep convective regions.

[66] As an indicator of the stability of $h_{mix/c}$ we calculated differences from $h_{mix/c}$, based not only on temperature profiles but also on salinity and potential density profiles.

The differences between the temperature and salinity $h_{mix/c}$ and those inferred from potential density profiles are smaller than 4 m on a global average, with no appreciable bias. This leads to an average uncertainty range of $h_{mix/c}$ about ±5 m for high- (<5 m) resolution profiles.

[67] A quality index, QI_{mix}, was introduced that determined whether a methodology would be able to cleanly separate the homogeneous layer depth from the stratified region below. In effect, it computes the anticorrelation between the stratification above and below the calculated mixed layer, with a value of 1.0 if no stratified water is above the depth of the mixed layer computation. $QI_{mix/c}$ was large (>0.7) for the bulk (>70%) of the profiles and supports the relatively small uncertainty range for $h_{mix/c}$ computed from high resolution profiles. The curvature algorithm was able to capture the depth of the quasi-homogeneous zone independent of the stratification below.

[68] The uncertainty range for the 20-m resolution profiles was estimated to be ±8 m. An additional problem of using these low-resolution profiles was that there appears to be an accumulation of h_{mix} estimates around each of the levels at which data is sampled. The exponential interpolation in our curvature-based algorithm was not able to completely bypass this accumulation. However, the algorithm does not exhibit accumulation at sampling levels during summer and fall in midlatitudes where large gradients between the mixed and the submixed layer occur. In the tropics, the accumulation problem persists. Assuming that $h_{mix/c}$ based on high-resolution profiles is the real h_{mix} the significant higher explained variance (squared correlation coefficient) indicates that $h_{mix/c}$ based on low-resolution profiles is more reliable than the corresponding $h_{mix/d}$.

[69] Temporal averaging of the profiles, before computing a homogeneous layer depth, systematically underestimates h_{mix}. Furthermore, it enhances the accumulation of h_{mix} around the sampling levels. This occurs because temporal averaging smoothes the vertical gradients and broadens the depth interval of the seasonal thermocline, which in turn reduces the sensitivity of computing the depth of the extreme curvature. We conclude that the main concerns in the computation of a reliable h_{mix} are not only low vertical resolution of the profiles, but also data sparseness so the average of h_{mix} did not equal h_{mix} from the ensemble average profile.

[70] With the data set at our disposal it was possible to determine the variability of $h_{mix/c}$ on seasonal-to-interannual scales in several ocean regions from observations alone. The absolute standard deviation of monthly mean $h_{mix/c}$ on the global scale for different seasons reflects the pattern of seasonal mean $h_{mix/c}$. The largest values (>50 m) of the absolute variability were in the mode and deep-water formation regions in both hemispheres in winter (and partly in the northern hemispheric spring) with large $h_{mix/c}$ and small values for small $h_{mix/c}$. The relative standard deviation of monthly mean $h_{mix/c}$ is most pronounced (>50%) in the eastern equatorial Pacific where there is a small monthly mean $h_{mix/c}$ and weak absolute variability throughout the year. This also reflects the high sensitivity of small $h_{mix/c}$ to variations caused by horizontal or vertical processes that move the thermocline by adiabatic processes. The relative standard deviation of $h_{mix/c}$ ranges between 20 and 70%.

[71] To highlight the effect of anomalous monthly mean $h_{mix/c}$ on the climate variability, we focused on the tropical Pacific and calculated the correlation between anomalous monthly mean $h_{mix/c}$ and SST; this correlation indicates that basically the variability of $h_{mix/c}$ on seasonal-to-interannual scales is decoupled from the anomalous SST changes. Therefore the processes that change the SST must be related more to horizontal movements of water masses than to processes of local storage of thermal energy.

[72] Analysis with ECCO simulated temperature profiles first of all revealed that the estimated $h_{mix/c}$ does follow the models true mixing depth, h_{pbl}, relatively close. This indicates that $h_{mix/c}$ is a good proxy for the models mixing depth and it appears to be a better estimate of h_{pbl} than the traditional $h_{mix/d}$. We found also a weaker correlation between h_{pbl} and $h_{mix/d}$ than for the corresponding $h_{mix/c}$. Comparisons of observed $h_{mix/c}$ with ECCO simulated $h_{mix/c}$ as well as with the *K*PP diagnosed oceanic planetary boundary layer depth h_{pbl} confirm that in the Pacific equatorial zone ECCO produced a weakly stratified upper layer more from assimilated T/T observations of temperature rather than from turbulence created by its imbedded *K*PP. The h_{pbl} was significantly smaller than the quasi-homogeneous layer depth in the ECCO simulations. Secondly, even though observed $h_{mix/c}$ was significantly larger than h_{pbl}, also in midlatitudes, there was a strong correlation between them on monthly anomaly timescales (>0.8). This implies either that the ECCO vertical diffusivity below the *K*PP planetary boundary layer plays an important role in diffusing heat from the mixed layer into the seasonal and main thermocline below, or that the correlation is set up by the ECCO assimilation of the same profiles we are using for verification. We found that a weaker correlation occurred between $h_{mix/d}$ and h_{pbl}.

[73] It goes without saying that we are looking very much forward to the profile data set generated from the ARGO project with which to further test the applicability of our, and other, mixed layer computations. However, if all the ARGO data is assimilated, model testing for upper ocean mixing via computation of mixed layer depth will be moot.

[74] **Acknowledgments.** This study benefited from a poster presentation at the WOCE and beyond conference in San Antonio, Texas, November 2002. We would like to thank the anonymous reviewer and James Richman for their valuable and helpful comments. In this respect we thank as well Johannes Karstensen. The paper was motivated by discussions with Russ Davis. Supported in part through ONR (NOPP) ECCO grants N00014-99-1-1049. This is a contribution of the Consortium for Estimating the Circulation and Climate of the Ocean (ECCO) funded by the National Oceanographic Partnership Program.

References

Alexander, M. A., and C. Deser (1995), A Mechanism for the Recurrence of Wintertime Midlatitude SST Anomalies, *J. Phys. Oceanogr.*, *25*, 122–137.

Alexander, M. A., J. D. Scott, and C. Deser (2000), Processes that influence sea surface temperature and ocean mixed layer depth variability in a coupled model, *J. Geophys. Res.*, *105*, 16,823–16,842.

Brainerd, K. E., and M. C. Gregg (1995), Surface mixed and mixing layer depths, *Deep Sea Res., Part I*, *42*(9), 1521–1543.

de Boyer Montégut, C., G. Mardec, A. S. Fischer, A. Lazar, and D. Iudicone (2004), Mixed layer depth over the global ocean: An examination of profile data and a profile based climatology, *J. Geophys. Res.*, *109*, C12003, doi:10.1029/2004JC002378.

Deser, C., M. A. Alexander, and M. S. Timlin (2003), Understanding the Persistence of the Sea Surface Temperature Anomalies in the Mid-latitudes, *J. Clim.*, *16*(1), 57–72.

Dommenget, D., and M. Latif (2002), Analysis of observed and simulated SST spectra in the mid-latitudes, *Clim. Dyn.*, *19*, 277–288.

Jin, F. F. (1997), An equatorial ocean recharge paradigm for ENSO. Part I: Conceptual model, *J. Atmos. Sci.*, *54*, 811–829.

Kalnay, E., et al. (1996), The NCEP/NCAR 40-Year Reanalysis Project, *Bull. Am. Meteorol. Soc.*, *77*, 437–471.

Kara, A. B., P. A. Rochford, and H. E. Hurlburt (2000a), Mixed layer depth variability and barrier layer formation over the North Pacific Ocean, *J. Geophys. Res.*, *105*, 16,783–16,801.

Kara, A. B., P. A. Rochford, and H. E. Hurlburt (2000b), An optimal definition for the ocean mixed layer depth, *J. Geophys. Res.*, *105*, 16,803–16,821.

Krahmann, G., et al. (2003), The Labrador Sea Deep Convection Experiment data collection, *Geochem. Geophys. Geosyst.*, *4*(10), 1091, doi:10.1029/2003GC000536.

Large, W. G., J. C. Williams, and P. P. Niiler (1986), Upper ocean thermal response to strong autumnal forcing of the northeast Pacific, *J. Phys. Oceanogr.*, *16*, 1524–1550.

Large, W. G., J. C. Williams, and S. C. Doney (1994), Oceanic vertical mixing: A review and a model with a non-local boundary-layer parameterization, *Rev. Geophys.*, *32*, 363–403.

Levitus, S., and T. P. Boyer (1994), *World Ocean Atlas 1994*, vol. 4, *Temperature*, *NOAA ATLAS NESDIS 4*, 129 pp., NOAA, Silver Spring, Md.

Levitus, S., R. Burgett, and T. P. Boyer (1994), *World Ocean Atlas 1994*, vol. 3, *Salinity*, *NOAA ATLAS NESDIS 3*, 111 pp., NOAA, Silver Spring, Md.

Lukas, R., and E. Lindstrom (1991), The mixed Layer of the western equatorial Pacific Ocean, *J. Geophys. Res.*, *96*, 3343–3357.

Menemenlis, D., I. Fukumori, and T. Lee (2005), Using Green's functions to calibrate an ocean general circulation model, *Mon. Weather Rev.*, *133*, 1224–1240.

Moisan, J. R., and P. P. Niiler (1998), The seasonal heat budget of the North Pacific: Net heat flux and storage rates (1950–1990), *J. Phys. Oceanogr.*, *28*(3), 401–421.

Niiler, P. P. (1982), FRONTS-80: A study of the North Pacific subtropical front, *Nav. Res. Rev.*, *34*(3), 41–52.

Reynolds, R. W., and T. M. Smith (1994), Improved global sea surface temperature analysis using optimum interpolation, *J. Clim.*, *7*, 929–948.

Roads, J., et al. (2003), GCIP water and energy budget synthesis (WEBS), *J. Geophys. Res.*, *108*(D16), 8609, doi:10.1029/2002JD002583.

Rudnick, D. L., and R. Ferrari (1999), Compensation of horizontal temperature and salinity gradients in the ocean mixed layer, *Science*, *283*, 526–529.

Speer, K. G., H. J. Isemer, and A. Biastoch (1995), Water mass formation revised from COADS data, *J. Phys. Oceanogr.*, *25*, 2444–2457.

Sprintall, J., and M. Tomczak (1992), Evidence of the barrier layer in the surface layer of the tropics, *J. Geophys. Res.*, *97*(C5), 7305–7316.

Talley, L. D., and M. E. Raymer (1982), Eighteen degree water variability, *J. Mar. Res.*, *40*, Suppl, 757–777.

Thomson, R. E., and I. V. Fine (2003), Estimating mixed layer depth from oceanic profile data, *J. Atmos. Oceanic Technol.*, *20*(2), 319–329.

Tomczak, M., and J. S. Godfrey (1994), *Regional Oceanography: An Introduction*, 442 pp., Elsevier, New York.

Wang, W., and M. J. McPhaden (2001), Surface layer temperature balance in the equatorial Pacific during the 1997–98 El Nino and 1998–99 La Nina, *J. Clim.*, *14*, 3393–3407.

World Ocean Circulation Experiment International Project Office, WOCE Data Products Committee (WOCE IPO) (2002), Global data resource version 3.0 [DVDs], *Rep. 180/02*, Southampton, U. K.

A. Köhl, Institut für Meereskunde, Düsternbrooker Weg 20, D-24105 Hamburg, Germany.

D. Dommenget and K. Lorbacher, IFM-GEOMAR, Düsternbrooker Weg 20, D-24105 Kiel, Germany. (ddommenget@ifm-geomar.de)

P. P. Niiler, Scripps Institution of Oceanography, 9500 Gilman Drive 0213, La Jolla, CA 92093-0213, USA.